Structural Insights Into the Initiation and Elongation of Ubiquitination by Ubr1

Authors:

Man Pan[1,4,*], Qingyun Zheng[2,4], Tian Wang[2,4], Lujun Liang[2,4], Junxiong Mao[2], Chong Zuo[2], Ruichao Ding[2], Huasong Ai[2], Yuan Xie[1], Dong Si[3], Yuanyuan Yu[1,*], Lei Liu[2,*], Minglei Zhao[1,*]

Affiliations:

[1] Department of Biochemistry and Molecular Biology, The University of Chicago; Chicago, IL 60637, USA.

[2] Tsinghua-Peking Center for Life Sciences, Department of Chemistry, Tsinghua University; Beijing 100084, China.

[3]Division of Computing and Software Systems, University of Washington Bothell, Bothell, WA 98011

[4]These authors contributed equally to the work.

*Corresponding authors:

Minglei Zhao. Email: mlzhao@uchicago.edu

Lei Liu. Email: lliu@mail.tsinghua.edu.cn

Yuanyuan Yu. Email: yuanyuanyu@uchicago.edu

Man Pan. Email: panm@uchicago.edu

Abstract

The N-end rule pathway was one of the first ubiquitin (Ub)-dependent degradation pathways to be identified. Ubr1, a single-chain E3 ligase, targets proteins bearing a destabilizing residue at the N-terminus (N-degron) for rapid K48-linked ubiquitination and proteasome-dependent degradation. How Ubr1 catalyses the initiation of ubiquitination on the substrate and elongation of the Ub chain in a linkage-specific manner through a single E2 ubiquitin-conjugating enzyme (Ubc2) remains unknown. Here, we report the cryo-electron microscopy structures of two complexes representing the initiation and elongation intermediates of Ubr1 captured using chemical approaches. In these two structures, Ubr1 adopts different conformations to facilitate the transfer of Ub from Ubc2 to either an N-degron peptide or a monoubiquitinated degron. These structures not only reveal the architecture of the Ubr1 complex but also provide mechanistic insights into the initiation and elongation steps of ubiquitination catalysed by Ubr1.

Keywords

Ubr1, Ubc2, degron, ubiquitination, N-end rule, chemical trapping, single-particle cryo-EM

37 **INTRODUCTION**

38 Ubiquitination is involved in a wide range of cellular processes, such as protein homeostasis,
39 cell cycle regulation, transcriptional regulation, and the stress response [1,2]. In particular, the N-
40 end rule pathway was the first specific pathway of the ubiquitin (Ub) system to be identified [3].
41 This pathway determines the rate of protein degradation through recognition of the N-terminal
42 residues termed N-degrons. In eukaryotes, N-degrons are recognized by specific ubiquitin
43 ligases (E3) followed by rapid polyubiquitination of a nearby lysine residue, which marks the
44 protein for degradation by the 26S proteasome [4-7]. It has been estimated that more than 80% of
45 human proteins can be regulated by the N-end rule pathway [8]. Misregulation of the N-end rule
46 pathway leads to the accumulation of unwanted proteins and proteotoxicity, which underlies
47 ageing and specific diseases, including neurodegeneration [9].

48 Three branches of the N-end rule pathway exist in eukaryotes, targeting N-terminal
49 arginine residues (Arg/N), proline residues (Pro/N), and acetyl groups (Ac/N) [10]. In
50 *Saccharomyces cerevisiae* (Baker's yeast), a single E3 ligase, Ubr1, is responsible for the
51 Arg/N-end pathway, which recognizes two types of N-degrons: one type starts with basic
52 residues (R, K, H), and the other starts with bulky hydrophobic residues (L, F, W, Y, I) [11]. By
53 contrast, in mammals, multiple Ubr1 homologues participate in the Arg/N-end pathway [12].
54 Human Ubr1 shares 20% sequence identity with yeast Ubr1 and is involved in the processes of
55 neurite outgrowth and axonal regeneration [13]. Mutations to human Ubr1 are associated with the
56 congenital disorder known as Johanson-Blizzard syndrome [9]. Ubr1 is a single-subunit RING-
57 type E3 ligase with a mass of over 200 kDa [14]. In vitro, yeast Ubr1 catalyses rapid K48-linked
58 polyubiquitination on substrate proteins that satisfy the N-end rule through the single E2
59 ubiquitin-conjugating enzyme Ubc2 (also known as Rad6) [11], which has been used to prepare
60 ubiquitinated substrates for in vitro assays [15]. Despite being discovered over 30 years ago [14],
61 the overall architecture of Ubr1 remains unknown. More importantly, how Ubr1 installs the first

62 Ub onto the substrate and the subsequent Ub molecules in an efficient and linkage-specific
63 manner remains to be elucidated. Due to the transient nature of the reaction intermediates,
64 visualization of this process is challenging.

65 Here, we developed chemical strategies to mimic the reaction intermediates of the first
66 and second Ub transfer steps catalysed by yeast Ubr1 and determined two cryo-electron
67 microscopy (cryo-EM) structures of Ubr1 in complex with Ubc2, Ub and either an N-degron
68 peptide or a ubiquitinated N-degron peptide, representing the initiation and elongation steps of
69 ubiquitination, respectively. The overall structures of these two complexes showed remarkable
70 resemblances to that of anaphase-promoting complex/cyclosome (APC/C), a highly conserved
71 multi-subunit E3 ligase involved in eukaryotic cell cycle regulation. Key structural elements,
72 including a Ubc2 binding region (U2BR) and an acceptor Ub binding loop on Ubr1, were
73 identified and characterized, which provided molecular insights into the initiation and elongation
74 steps of ubiquitination catalysed by Ubr1. Ubiquitination underlies many fundamental cellular
75 processes and is also critical for the development of novel therapeutic strategies, such as
76 proteolysis-targeting chimera (PROTAC) [16,17]. Our chemical approaches provide a general
77 strategy for the structural characterizations of other systems.

78

RESULTS

Previous work has shown that an Arg/N-degron peptide consisting of 43 amino acids can be polyubiquitinated at a Lys residue with K48 linkages [15]. We first synthesized the degron peptide (hereafter referred to as Degron) and a monoubiquitinated Degron (hereafter referred to as Ub-Degron) using solid phase peptide synthesis (**Fig. S1a & b**). For Ub-Degron, the native isopeptide bond was introduced by using a side chain-modified Lys residue through solid phase peptide synthesis. Subsequently, hydrazide-based native chemical ligation (NCL) was conducted to place Ub onto the Lys side chain [18] (**Fig. S1b**). To monitor the polyubiquitination reaction, we further labelled both Degron and Ub-Degron with fluorescein-5-maleimide (**Fig. S1c & d**) and confirmed their reactivity in a K48 linkage-specific manner with Ubr1 and Ubc2 in vitro (**Fig. S1e**). Next, we performed single-turnover ubiquitination reactions using Ubc2 loaded with mutant Ub (K48R) at a saturating concentration. The estimated K_m and K_{cat} for Degron were 1.24 ± 0.69 μM and 0.27 ± 0.07 min^{-1}, respectively, which represents the initiation step catalysed by Ubr1 (**Fig. S1f**). The single-turnover ubiquitination of Ub-Degron, representing the first elongation step catalysed by Ubr1, showed slightly slower kinetics with an estimated K_m of 1.63 ± 0.69 μM and K_{cat} of 0.17 ± 0.02 min^{-1} (**Fig. S1g**). Notably, this behaviour was different from that of multi-subunit cullin-RING ubiquitin ligase (CRL)-mediated ubiquitination, which is a two-step process involving a slow initiation step followed by rapid K48-specific chain elongation [19,20].

To capture the initiation step of ubiquitination catalysed by Ubr1, we synthesized a stable complex of Ubc2, Ub and Degron that mimicked the reaction intermediate (**Fig. 1a and Fig. S2a**). A similar design was used in recent studies of the SCF-E3 complex; however, in this work, the Ub moiety was conjugated to the natural ε-amino group of K17 in Degron instead of being directly fused to the N-terminus of the substrate [21,22]. This stable intermediate mimic was then mixed with Ubr1 in a 1:1.5 molar ratio and incubated on ice for 30 minutes followed by

104 vitrification and single-particle cryo-EM analysis (**Fig. S2c**). A dataset of 10,592 movie stacks
105 was collected and processed following the established workflow in RELION [23] (**Fig. S3a**). The
106 final reconstructed map had an overall resolution of 3.3 Å, allowing for de novo model building
107 (**Figs. S3b, 3c, & 4a; Table S1**). Ubr1 is a single-subunit E3 ligase with more than 1,900 amino
108 acids (**Fig. 1b**). Only the Ubr-Box1 structure was determined previously [24]. To overcome the
109 difficulty during model building, we used the artificial intelligence (AI)-based do novo modelling
110 tool DeepTracer [25] to build a starting model of the entire complex (see Methods for details) and
111 manually adjusted and refined the model using COOT [26]. The final model was refined in real
112 space using PHENIX [27] (**Table S2**).

113 The overall structure of the initiation complex, named Ubr1-Ubc2-Ub-Degron, adopted a
114 sailboat-like shape, bearing high resemblance to APC/C [28,29], although Ubr1-Ubc2-Ub-Degron
115 was much smaller at 120 Å × 120 Å × 65 Å (**Fig. 1c**). The hull of the "boat" is a large helical
116 scaffold (white-grey) interspaced by three domains: Ubr-Box1 (dark purple), Ubr-Box2 (light
117 blue), and a winged helical domain (dark blue). The helical scaffold is reminiscent of similar
118 bundle repeats found in other E3 ligases, especially the cullin proteins in CRLs [21,22,30]. We
119 further defined four regions of the helical scaffold based on the interspaced domains (**Fig. 1b,**
120 **Fig. S5a & b**). Only the structure of Ubr-Box1 has been previously reported [24]. The other
121 domains were identified using SWISS-MODEL [31]. The front of the "boat" is where the Ub-loaded
122 Ubc2 is recruited. Ubc2 is primarily bound by a single helix of Ubr1, termed the Ubc2 binding
123 region (U2BR, dark green, **Fig. 1b & c**). A RING finger domain (cyan) follows U2BR and
124 interacts with Ubc2 and the loaded Ub (**Fig. S5d**). A new helical domain termed the cap helical
125 domain (pink) follows the RING finger domain (**Fig. S5c**). The cap helical domain adopted a
126 new fold that did not give similar hits from the DALI server for protein structure comparison [32].
127 Finally, the UBLC domain (UBR/Leu/Cys domain) [33] (orange) acts like the mast of the "boat" by
128 interacting with Ubr-Box1 and the winged helical domain through a zinc-binding site (**Fig. 1c &**

129 **f**). Quadruple mutations of the residues involved in this interface (H161A, Y933A, D1175A, and
130 H1763A) greatly impaired the activity of Ubr1 (**Fig. 1f, Fig. S5f**).

131 The first three residues (RHG) of the Degron peptide were resolved bound to the designated
132 pocket of Ubr-Box1 (**Fig. 1d, Figs. S4a & 5e**) [24]. The active site of Ub transfer is ~35 Å away
133 from the C-terminus of Gly3, where Lys17 forms an isopeptide bond with the C-terminal Cys76
134 of Ub (**Fig. 1e**). The thirteen residues between Lys17 and Gly3 were not resolved, but the
135 distance between them indicated an extended conformation (2.7 Å/residue). Meanwhile, a
136 disulfide bond was formed between the cysteine and the active site of Ubc2 (Cys88), as
137 designed (**Fig. 1e**). Ub is on the backside of the complex and interacts with one of the zinc-
138 binding sites in the RING finger domain through the Ile36 patch (**Fig. S5d**). In addition, the
139 U2BR of Ubr1 forms an extensive interface with the backside of Ubc2 (**Fig. 1c**), reminiscent of
140 the Ube2g2 binding region (G2BR) in Gp78, an E3 ligase involved in endoplasmic reticulum-
141 associated degradation (ERAD) [34], and the Ubc7 binding region (U7BR) in Cue1p, a component
142 of several E3 complexes involved in ERAD [35]. Together, the noncovalent interactions between
143 Ubr1, Ubc2, and Ub position the Ubc2~Ub thioester bond for nucleophilic attack by Lys17 on
144 Degron. In summary, this complex structure shows how Ubr1 recruits Ubc2~Ub and facilitates
145 the transfer of Ub to a specific Lys residue on the Degron peptide; that is, the initiation step.

146 Once the first Ub is installed on the substrate, the subsequent elongation of the Ub chain cannot
147 occur without rearrangement of the structure. To understand the process and capture the
148 intermediate state of the elongation step, we designed another stable complex mimicking the
149 transition state (**Fig. 2a**). The C-terminus of donor Ub was linked to both Cys88 of Ubc2 (active
150 site) and C48 of acceptor Ub on Ub-Degron (**Fig. 2a** inset). Ubc2 was first chemically modified
151 with the bifunctional adaptor molecule **1** [36] at the catalytic Cys to form molecule **2**.
152 Subsequently, the S-acetamidomethyl (Acm) group on molecule **2** was removed to expose a β-
153 mercaptoethylamine group for NCL with a Ub thioester (Ub-MesNa) [36], generating Ubc2~Ub

154 carrying an additional thiol group (molecule **3**). Finally, a stable intermediate mimic was
155 obtained by the creation of a disulfide bond between the thiol groups of molecule **3** and a Ub-
156 Degron carrying the K48C point mutation (**Fig. 2b, Fig. S2b**). The intermediate mimic was then
157 mixed with Ubr1 in a 1:1.5 molar ratio and incubated on ice for 30 minutes, followed by
158 vitrification and single-particle cryo-EM analysis (**Fig. S2c**). A dataset of 5083 movie stacks was
159 collected and processed (**Fig. S6a**). The final reconstructed map had an overall resolution of 3.6
160 Å (**Fig. S6b & c**). Model building was performed by first docking the structure of the initiation
161 complex (Ubr1-Ubc2-Ub-Degron), followed by rigid-body adjustment in Chimera and manual
162 adjustment in COOT [26]. The final model was refined in real space using PHENIX [27] (**Table S2**).

163 The overall structure of the elongation complex, named Ubr1-Ubc2-Ub-Ub-Degron, adopted a
164 sailboat-like shape similar to that of Ubr1-Ubc2-Ub-Degron (**Fig. 2c**). The linker molecule
165 covalently linked to C88 of Ubc2 forms a disulfide bond with C48 of acceptor Ub and a peptide
166 bond with G75 of donor Ub, as designed (**Fig. 2d**). The acceptor Ub binds to the helical scaffold
167 of Ubr1 at a loop (678-681) located in region C (**Fig. 2e**), which was disordered in the initiation
168 complex (**Fig. 1c**). The acceptor Ub further participated in the recruitment of Ubc2~Ub by
169 binding at a new interface on Ubc2 (**Fig. 2f**). When mutations were introduced into the Ub
170 binding loop (678-681) on Ubr1 and the new interface (N123 and V124) on Ubc2, the
171 polyubiquitination level on Degron and Ub-Degron were greatly reduced compared to that of the
172 wild-type (**Fig. S7a & b**). Importantly, the Ub binding loop mutant transferred more Ub to Degron
173 than to Ub-Degron, suggesting that the elongation step was impaired (**Fig. S7a**). We further
174 examined the single-turnover ubiquitination of the Ub binding loop mutant using Ubc2 charged
175 with either wild-type Ub or mutant Ub with all lysines mutated to arginines (**Fig. S7c**). Much
176 higher Ub discharge was observed for Degron than Ub-Degron. These results suggested a
177 crucial role of the Ub binding loop on Ubr1 in the elongation step.

178 In addition to the new interacting surfaces on Ubr1 and Ubc2, U2BR and Ubc2 (including the
179 donor Ub) underwent a displacement of approximately 18 Å, whereas the relative positions of
180 other domains on Ubr1 remained unchanged (**Fig. 2g and Fig. S7d & e**). This displacement of
181 U2BR and Ubc2 repositioned the presumed thioester bond between Ubc2 and the donor Ub so
182 that this bond was approachable by the K48 of the acceptor Ub on Ub-Degron (**Fig. 2d & g**).
183 Together, the two complex structures suggested that the displacement of U2BR on Ubr1 is the
184 key to accommodating extra Ub molecules during the transition from the initiation step to the
185 elongation step.

186 We further investigated the extensive binding interface between U2BR and Ubc2 which remains
187 the same in both initiation and elongation complex (823.3 $Å^2$, **Fig. 3a & b**). Mutations of
188 interface residues either on U2BR (F1190A, Q1186A, F1183A, H1175A) or Ubc2 (L29A, P30A,
189 N37A, W149A) severely impacted the activity of Ubr1 (**Fig. 3f**). Almost no ubiquitination of
190 Degron was observed when including both mutants. We further synthesized a U2BR peptide
191 (Ubr1 1165-1200) and performed an in vitro ubiquitination reaction in the presence of the free
192 U2BR peptide, and dose-dependent inhibition of polyubiquitination was observed (**Fig. 3g**).
193 Using isothermal titration calorimetry (ITC), we quantified the affinity between the U2BR peptide
194 and Ubc2. The dissociation constant (*Kd*) was 143 (±45) nM (**Fig. S8a**). The effect of E1-
195 dependent thioester bond (Ubc2~Ub) formation in the presence of the U2BR peptide was also
196 examined. Interestingly, an inhibitory effect (IC50 = 9.75 ± 4.34 μM) was observed (**Fig. S8b &**
197 **c**), which was different from the activation effects of U7BR on Ubc7 [35] and the rate-decreasing
198 effects of G2BR on UBE2G2 [34]. We further tested the accessibility of the catalytic cysteine
199 (Cys88) of Ubc2 using a bulky fluorescent alkylation reagent (BFAR), fluorescein-5-maleimide,
200 in the presence of the U2BR peptide. The results suggested that the U2BR peptide did not
201 enhance the accessibility of this cysteine residue (**Fig. 3h**).

202 In both the initiation and elongation structures, we observed smaller interfaces between Ubc2
203 and the RING finger domain of Ubr1 (410.3 Å^2 and 208.2 Å^2, respectively) than were observed
204 in previous studies, such as the interface between UbcH5 (E2) and the RING domain of TRIM25
205 (547.4 Å^2, PDB: 5FER, **Fig. 3c-e**) [37], although the so-called closed conformation of the E2 and
206 Ub subcomplexes remained the same. Indeed, mapping of conserved E2 residues involved in
207 the RING-E2 interaction showed that Ubc2 does not have the highly conserved aromatic Phe
208 residue involved in the interface, which has been shown to be important for activity [38]. In yeast
209 and human Ubc2, this residue is mutated to asparagine (**Fig. 3i**). As expected, the N65F
210 mutation of Ubc2 decreased ubiquitination activity in vitro (**Fig. 3j**), suggesting that this Phe
211 residue is not required for the interaction between Ubc2 and the RING finger domain of Ubr1.
212 Interestingly, the N65A mutation increased the amount of polyubiquitinated Degron (**Fig. 3j**),
213 suggesting that N65 may not be important for the elongation of Ubr1-mediated ubiquitination.
214 Notably, the interface between Ubc2 and the RING domain changed in the elongation structure.
215 A conserved tryptophan residue (W96 of Ubc2) flipped out and interacted with the RING domain
216 instead of N65 (**Fig. 3d & i**). The W96A mutation did not affect the initiation step but severely
217 decreased the amount of polyubiquitinated Degron (**Fig. 3j**). This result suggested that the new
218 interface involving the tryptophan residue is critical for the elongation of Ub chain and may play
219 a role in other E2-E3 systems.

220

221 **DISCUSSION**

222 Visualizing E3-mediated substrate ubiquitination is of great importance [39], and it is also
223 informative for the development of novel therapeutic strategies such as PROTAC [16,17]. The
224 chemical trapping of ubiquitinated intermediates has played critical roles in the mechanistic
225 understanding of various E3 ligases. The Lima group engineered an E2 to trap the $E3_{Siz1}/E2_{Ubc9}$-
226 SUMO/PCNA complex, demonstrating that E3 could bypass E2 specificity to force-feed a
227 substrate lysine into the E2 active site [40]. The Schulman group designed a chemically trapped
228 complex of neddylated $CRL1^{\beta\text{-}TRCP}$-UBE2D-Ub-phosphorylated IκBα, showing that the E3 ligase
229 $CRL1^{\beta\text{-}TRCP}$ primed and positioned Ub and the substrate lysine for transfer [38]. Here, through the
230 chemical synthesis of two ubiquitination intermediate mimics representing the initiation and
231 elongation steps and single-particle cryo-EM analysis, we revealed the mechanism of Ubr1-
232 mediated ubiquitination involved in the N-end rule pathway. Our cryo-EM structures suggested
233 the rapid and linkage-specific ubiquitination of Ubr1 (**Fig. 4**). Specifically, substrates bearing
234 destabilizing amino-terminal degrons are captured by Ubr1 through the Ubr-Box. Ub-charged
235 E2, Ubc2~Ub, is recruited through the U2BR and the RING domain. The positions of these
236 domains on Ubr1 facilitate Ub thioester transfer to a Lys residue near the degron (initiation
237 step). The helical scaffold of Ubr1 provides an additional anchor (the Ub binding loop) for Ub on
238 the newly formed monoubiquitinated substrate. Ub also participates in the rearrangement of
239 U2BR-Ubc2 by interacting with a new interface on Ubc2. The specific binding between the Ub
240 binding loop and Ub ensures close proximity of K48 on Ub and the newly formed thioester bond
241 at the active site of Ubc2, which facilitates the transfer of the second Ub (elongation step). We
242 further speculate that similar rearrangements occur for subsequent elongation steps. The most
243 distal Ub is always engaged by the Ub binding loop on Ubr1 to ensure linkage specificity of the
244 polyubiquitin chain (**Fig. 4**).

245 Our structures revealed that U2BR plays a key role in the recruitment of Ubc2. Notably, single-
246 particle analysis of Ubr1 alone showed that the cap helical domain was very flexible without
247 Ubc2 and the substrate (**Fig. S9**). U2BR could not be resolved from 2D class averages and 3D
248 reconstruction, suggesting that the chemical synthesis of intermediate mimics is the key to
249 stabilizing Ubr1, which leads to structure determination at near-atomic resolution. The strategies
250 presented in this study can be adopted to investigate the mechanism of other E3 ligases.

251 In humans, Johanson-Blizzard syndrome is a rare and severe autosomal recessive genetic
252 disorder caused by mutations to Ubr1 [9]. Human Ubr1 shares 20% sequence identity with the
253 yeast homologue, especially in Ubr-Box1, Ubr-Box2, region C of the helical scaffold, the U2BR
254 and the RING finger domain. Given the similarity, human Ubr1 is very likely to have a similar
255 mechanism. Our structures provide a molecular basis to understand the pathogenesis of this
256 disease.

257

ACKNOWLEDGEMENTS

We thank the staff at the National Cryo-Electron Microscopy Facility at the Frederick National Laboratory and the Advanced Electron Microscopy Facility at the University of Chicago for the help in cryo-EM data collection. Funding: Funding for this work was, in part, provided by the Catalyst Award from the Chicago Biomedical Consortium. This work was supported by Chicago Biomedical Consortium Catalyst Award C-086 to M.Z. We thank the National Key R&D Program of China (No. 2017YFA0505200), NSFC (91753205) for financial support. This research was, in part, supported by the National Cancer Institute's National Cryo-EM Facility at the Frederick National Laboratory for Cancer Research under contract HSSN261200800001E. This material is based upon work supported by the National Science Foundation under Grant No. 2030381, the graduate research award of Computing and Software Systems division, and the start-up fund 74–0525 at University of Washington Bothell to D.S.. Any opinions, findings, and conclusions or recommendations expressed in this material are those of the authors and do not necessarily reflect the views of the National Science Foundation. Molecular graphics and analyses were performed with UCSF ChimeraX, developed by the Resource for Biocomputing, Visualization, and Informatics at the University of California, San Francisco, with support from National Institutes of Health R01-GM129325 and the Office of Cyber Infrastructure and Computational Biology, National Institute of Allergy and Infectious Diseases.

AUTHOR CONTRIBUTIONS

M.P., M.Z., L.L. and Y.Y. designed all the experiments and interpreted the results. M.P., Q.Z. and L. L. designed the synthetic route for chemically synthesized ubiquitination initiation and elongation intermediate mimics. T.W. synthesized the fluorescently labelled Ub-Degron and the elongation intermediate mimic. L.J.L. synthesized the fluorescently labelled Degron and the initiation intermediate mimic. M.P., Y.Y., D.S., and M.Z. performed cryo-EM data collection and

processing. J.M. performed the in vitro ubiquitination assays with Ubr1 and Ubc2 mutants. Q.Z. performed characterization of the U2BR peptide on the enzymatic properties of Ubc2. T.W., Y.Y., R.D., J.M., H.A. and Y.X. cloned, expressed, and purified Ubr1, Ubc2 and their mutants. M.Z., M.P., and L.L. wrote the paper. M.Z., L.L., Y.Y. and M.P. supervised the project.

COMPETING INTERESTS

The authors declare no competing interests.

289 **Figure Legends**

290 **FIG. 1**

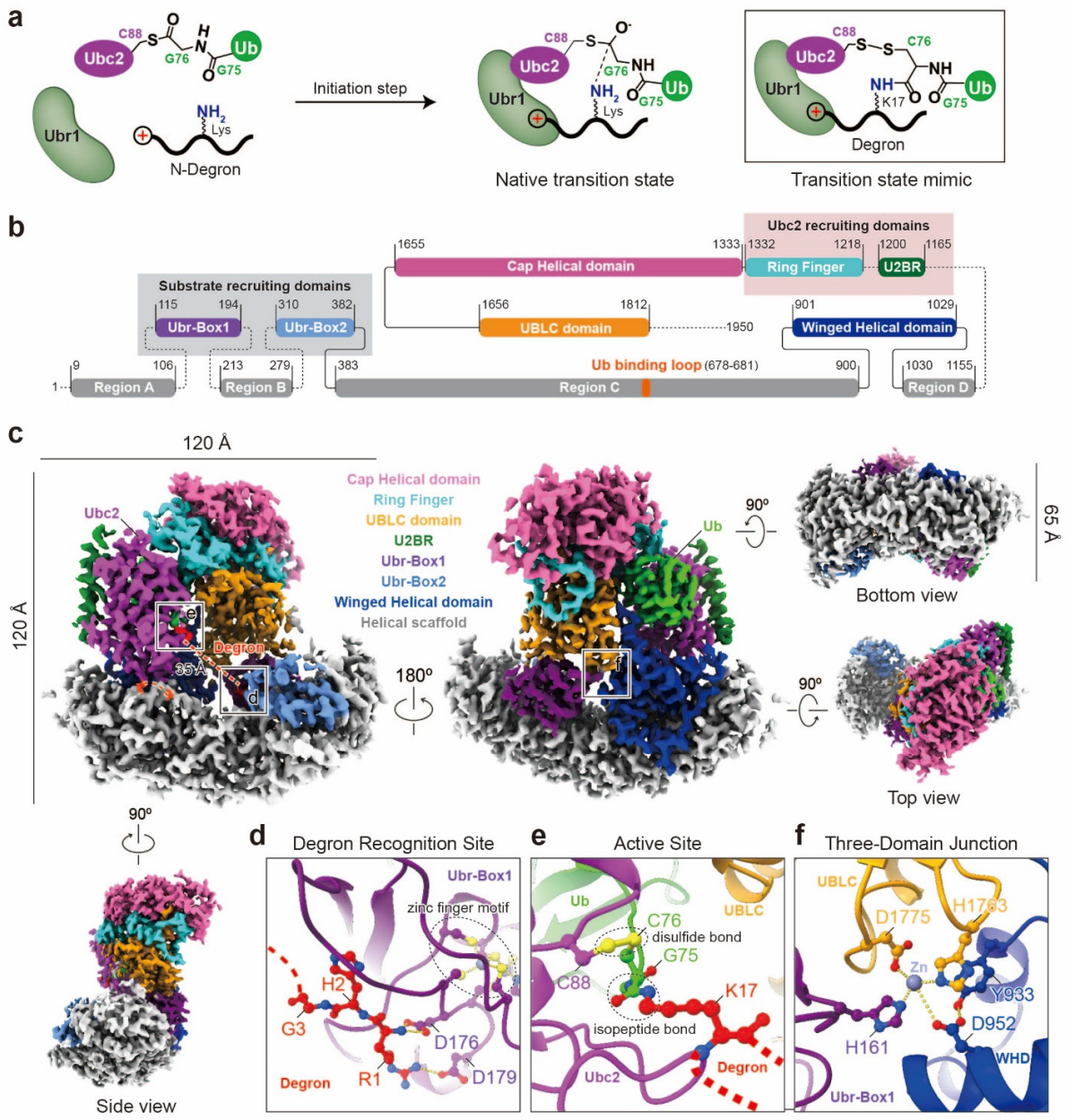

291

292

293

294 **Figure 1: Structure of the initiation complex.**

295 **a**, A schematic representation of the transition state of the initiation step. The side chain of a Lys
296 residue on Degron attacks the thioester bond of Ubc2~Ub. The inset shows the designed
297 intermediate structure mimicking the transition state of the initiation step. **b**, A schematic domain
298 diagram of Ubr1, with residue boundaries indicated. Dotted lines represent unresolved linkers
299 and regions. **c**, Cryo-EM maps of the initiation complex (sharpened using a B factor of -96.5 $Å^2$,
300 contour level: 0.03). The colour code of Ubr1 is the same as that in panel **b**. **d,** Molecular
301 interactions between Degron and Ubr-Box1. Hydrogen bonds and electrostatic interactions are
302 represented by dotted lines. **e,** Molecular structure of the active site. **f,** Molecular interactions
303 between UBLC, Ubr-Box1 and the winged helical domain (WHD). Metal coordination bonds and
304 hydrogen bonds are represented by dotted lines. Mutations of the four residues at the interface
305 (H161, Y933, H1763 and D1775) impaired the activity of Ubr1.

306

307 **FIG. 2**

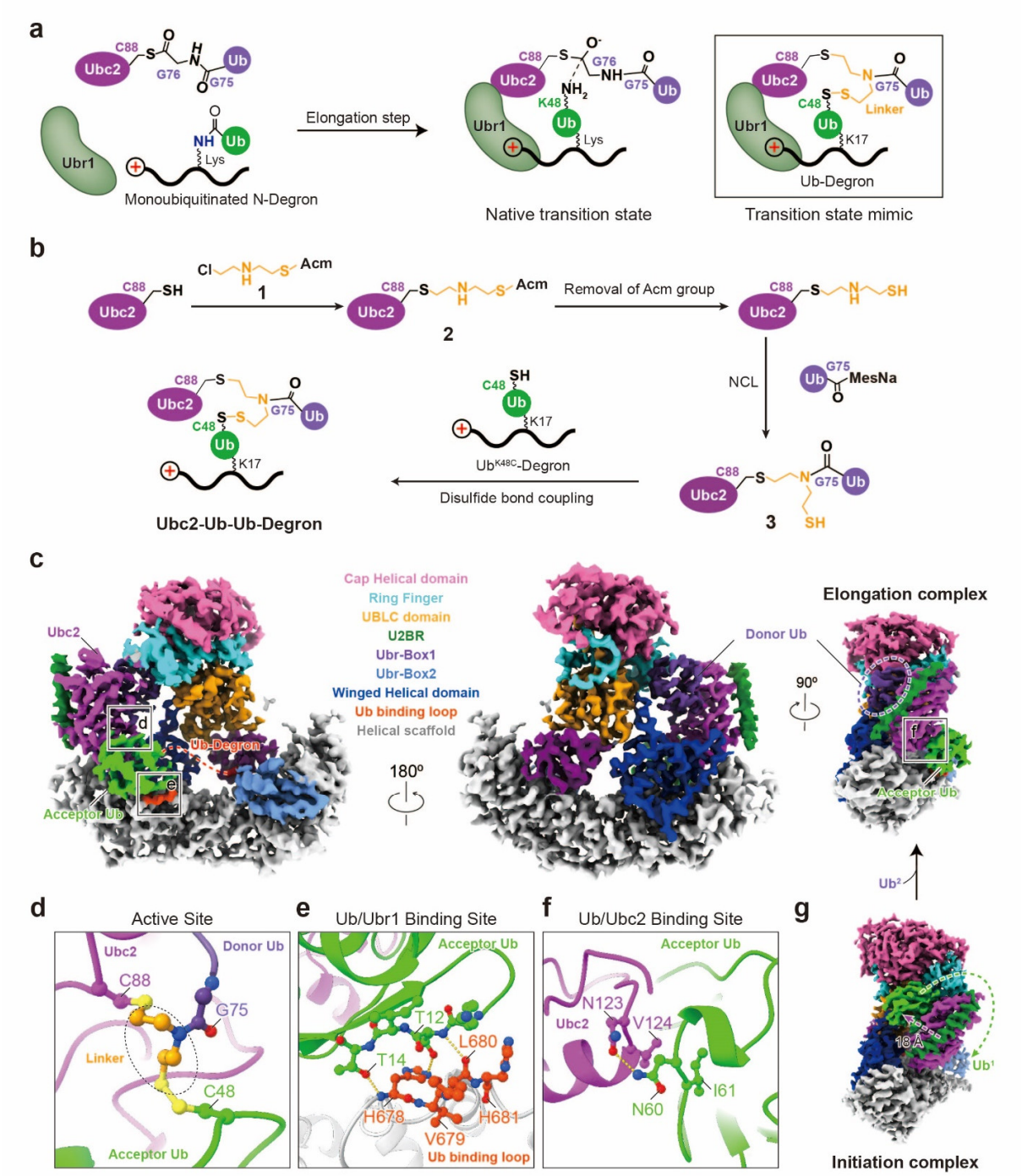

308

309

310 **Figure 2: Structure of the elongation complex.**

311 **a**, A schematic representation of the transition state of the elongation step. The side chain of
312 K48 on Ub-Degron attacks the thioester bond of Ubc2~Ub. The inset shows the designed
313 intermediate structure mimicking the transition state of the elongation step. **b**, The synthetic
314 route of the intermediate structure mimicking the transition state of the elongation step. **c**, Cryo-
315 EM maps of the elongation complex (sharpened using a B factor of -96.7 $Å^2$, contour level:
316 0.022). The colour code of Ubr1 is the same as that in Fig. 1**b**. **d,** Molecular structure of the
317 active site. **e,** Molecular interactions between acceptor Ub and the Ub binding loop of Ubr1.
318 Hydrogen bonds are represented by dotted lines. **f,** Molecular interactions between acceptor
319 Ub and Ubc2. Hydrogen bonds are represented by dotted lines. **g**, A side view of the initiation
320 complex in the same orientation as that of the elongation complex in panel **c**. Displacement of
321 Ubc2, U2BR, and Ub are noted with arrows.

322

FIG. 3

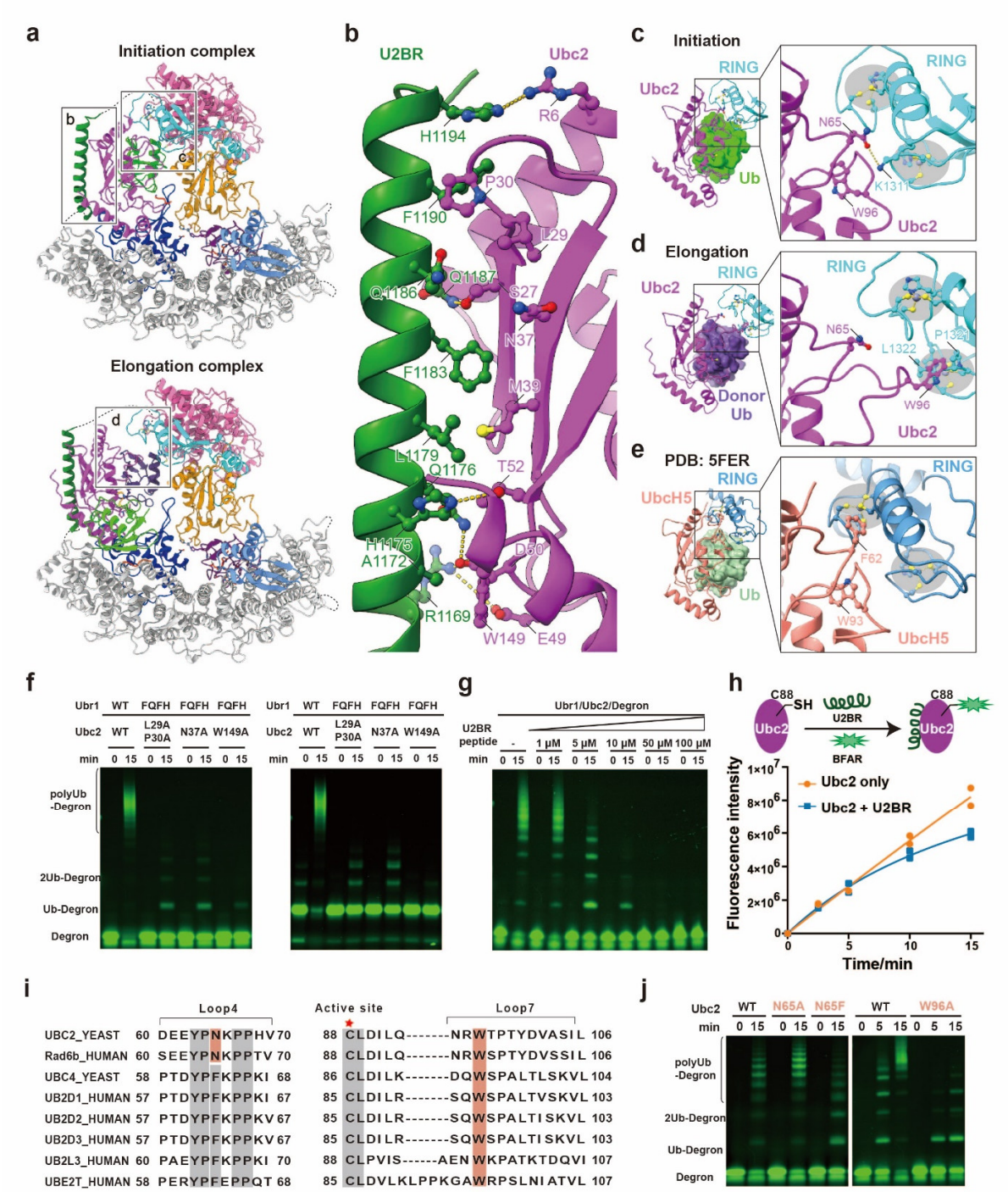
a
Initiation complex
Elongation complex
b
U2BR
Ubc2
H1194
R6
P30
F1190
L29
Q1187
Q1186
S27
N37
F1183
M39
L1179
Q1176
T52
H1175
A1172
D50
R1169
W149
E49
c
Initiation
RING
Ubc2
Ub
N65
K1311
W96
d
Elongation
Donor Ub
L1322
P1321
e
PDB: 5FER
UbcH5
F62
W93
f
Ubr1
WT
FQFH
Ubc2
L29A P30A
N37A
W149A
min
polyUb -Degron
2Ub-Degron
Ub-Degron
Degron
g
Ubr1/Ubc2/Degron
U2BR peptide
1 μM
5 μM
10 μM
50 μM
100 μM
h
C88
SH
U2BR
BFAR
Ubc2 only
Ubc2 + U2BR
Fluorescence intensity
Time/min
i
Loop4
Active site
Loop7
UBC2_YEAST 60 DEEYPNKPPHV 70 88 CLDILQ-------NRWTPTYDVASIL 106
Rad6b_HUMAN 60 SEEYPNKPPTV 70 88 CLDILQ-------NRWSPTYDVSSIL 106
UBC4_YEAST 58 PTDYPFKPPKI 68 86 CLDILK-------DQWSPALTLSKVL 104
UB2D1_HUMAN 57 PTDYPFKPPKI 67 85 CLDILR-------SQWSPALTVSKVL 103
UB2D2_HUMAN 57 PTDYPFKPPKV 67 85 CLDILR-------SQWSPALTISKVL 103
UB2D3_HUMAN 57 PTDYPFKPPKV 67 85 CLDILR-------SQWSPALTISKVL 103
UB2L3_HUMAN 60 PAEYPFKPPKI 70 88 CLPVIS------AENWKPATKTDQVI 107
UBE2T_HUMAN 58 PERYPFEPPQT 68 85 CLDVLKLPPKGAWRPSLNIATVL 107
j
Ubc2
WT
N65A
N65F
W96A
min
polyUb -Degron
2Ub-Degron
Ub-Degron
Degron

326 **Figure 3: Analysis of the interactions between Ubc2 and Ubr1.**

327 **a**, Molecular structures of the initiation complex and the elongation complex. **b**, A close-up view
328 of the interface between Ubc2 and the U2BR of Ubr1. Labelled residues are involved in
329 extensive noncovalent interactions. Hydrogen bonds and electrostatic interactions are
330 represented by dotted lines. **c-e**, Close-up views of the interface between E2 and RING finger
331 domains. **c,** Ubc2 and the RING finger domain in the initiation complex. Hydrogen bonds are
332 represented by dotted lines. **d,** Ubc2 and the RING finger domain in the elongation complex. **e,**
333 UbcH5 and the RING finger domain of TRIM25 (PDB: 5FER) [38]. **f-g**, In vitro Ubr1-dependent
334 ubiquitination assays. **f,** Ubr1 and Ubc2 mutants at the interface shown in panel **b** were tested.
335 **g**, The inhibition of Ubr1-dependent ubiquitination in the presence of increasing concentrations
336 of a synthetic U2BR peptide. **h**, The accessibility of the catalytic cysteine (Cys88) of Ubc2
337 tested using a BFAR in the presence or absence of the synthetic U2BR peptide. The average
338 fluorescence from two independent experiments was plotted. **i**, Sequence alignment of multiple
339 E2 enzymes, including yeast and human Ubc2 (also known as Rad6b). Two regions involved in
340 the interaction with the RING finger domain are shown. **j**, In vitro Ubr1-dependent ubiquitination
341 assays investigating the role of N65 and W96 of Ubc2 in the interaction with the RING finger
342 domain of Ubr1.

343 **FIG. 4**

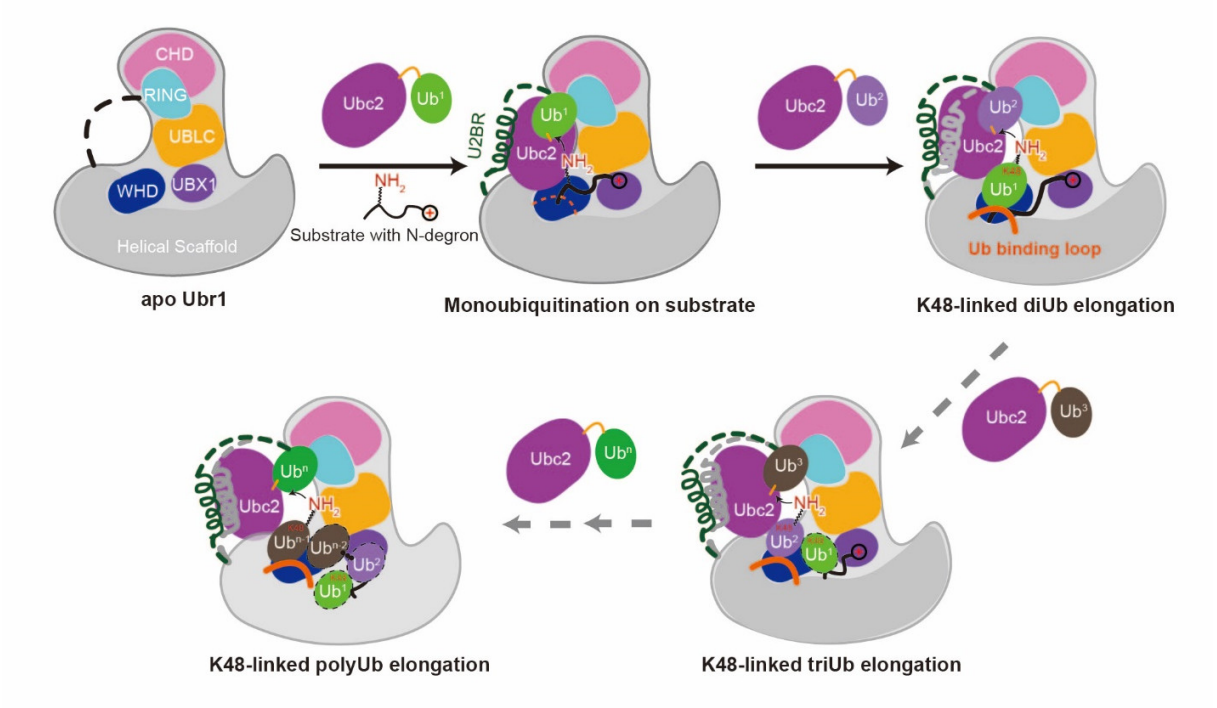

344

345

346 **Figure 4: Model of Ubr1-mediated polyubiquitination.**

347 A cartoon representation of Ubr1-mediated polyubiquitination starting from a degron peptide
348 with a positively charged N-terminal residue. The first two steps correspond to the initiation and
349 elongation structures described in this study. Subsequent elongation of the polyubiquitin chain is
350 hypothetical. The Ub molecules being conjugated are sequentially numbered as Ub^1, Ub^2, …,
351 Ub^n.

352

353 **Supplementary Figures and Legends**

354 **FIG. S1**

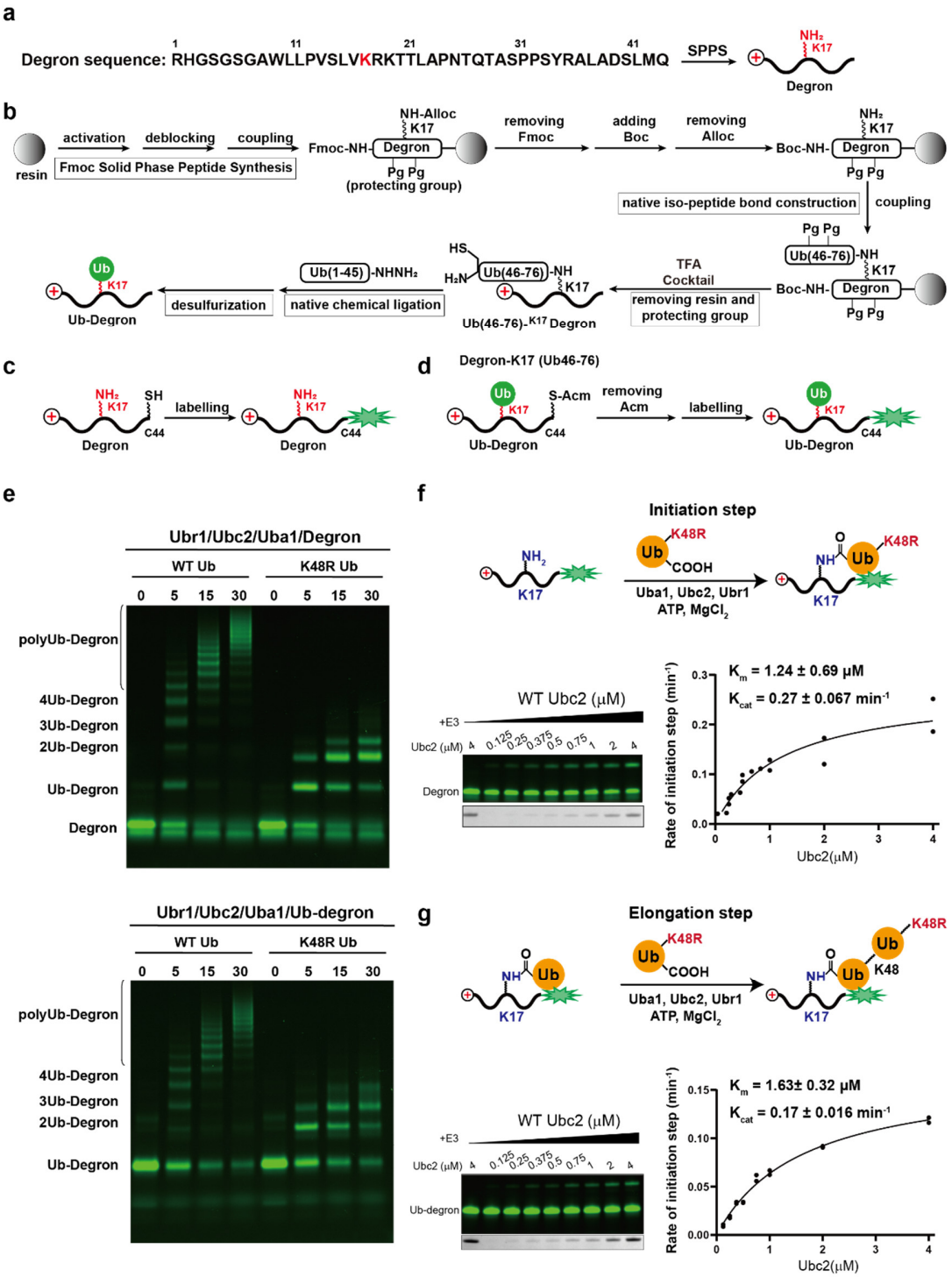

355

356 **Fig. S1: Ubr1-mediated K48-linked polyubiquitination of degron peptides.**

357 **a**, Amino acid sequence of the degron peptide (Degron). **b**, The synthetic route of the
358 monoubiquitinated degron peptide (Ub-Degron). **c-d**, Fluorescent labelling of Degron (**c**) and
359 Ub-Degron (**d**). **e**, In vitro Ubr1-dependent ubiquitination assays using fluorescent Degron (top)
360 and Ub-Degron (bottom) as substrates. **f-g**, Quantitative evaluation of the Ubr1 enzyme kinetics
361 for ubiquitination initiation (**f**) and the first step of elongation (**g**). Averages of two independent
362 experiments were plotted and fit to the Michaelis–Menten model to estimate the K_m and K_{cat}.

363

364 **FIG. S2**

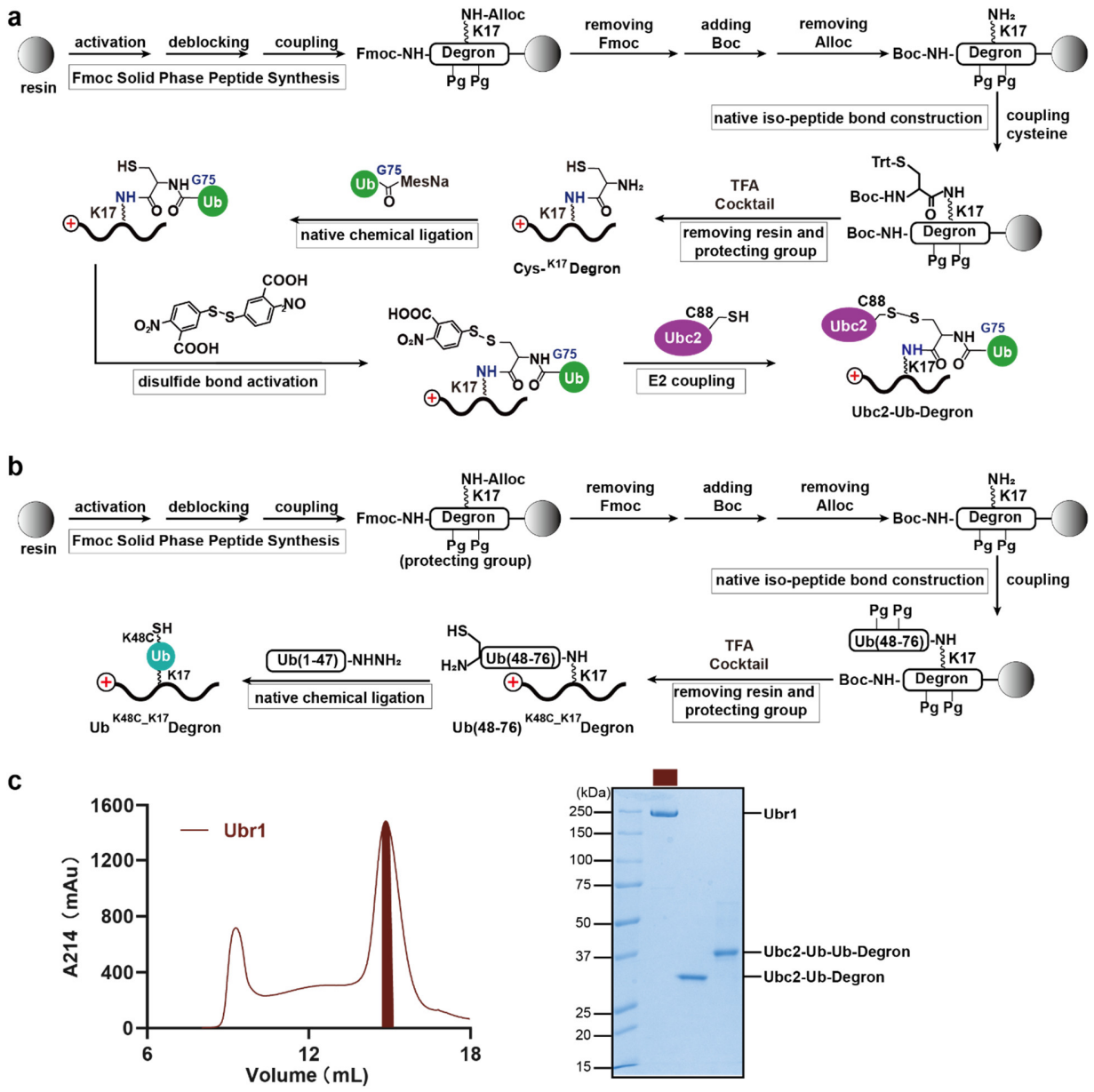

365

366

367 **Fig. S2: Synthesis and purification of the intermediate structures.**

368 **a**, The synthetic route of the designed structure mimicking the transition state of the initiation

369 step. **b**, The synthetic route of Ub(K48C)-^{K17}Degron. **c**, A gel filtration chromatogram of Ubr1

370 (left) and an SDS-PAGE gel of purified Ubr1 and designed stable intermediate structures Ubc2-
371 Ub-Degron and Ubc2-Ub-Ub-Degron (right).
372

373 **FIG. S3**

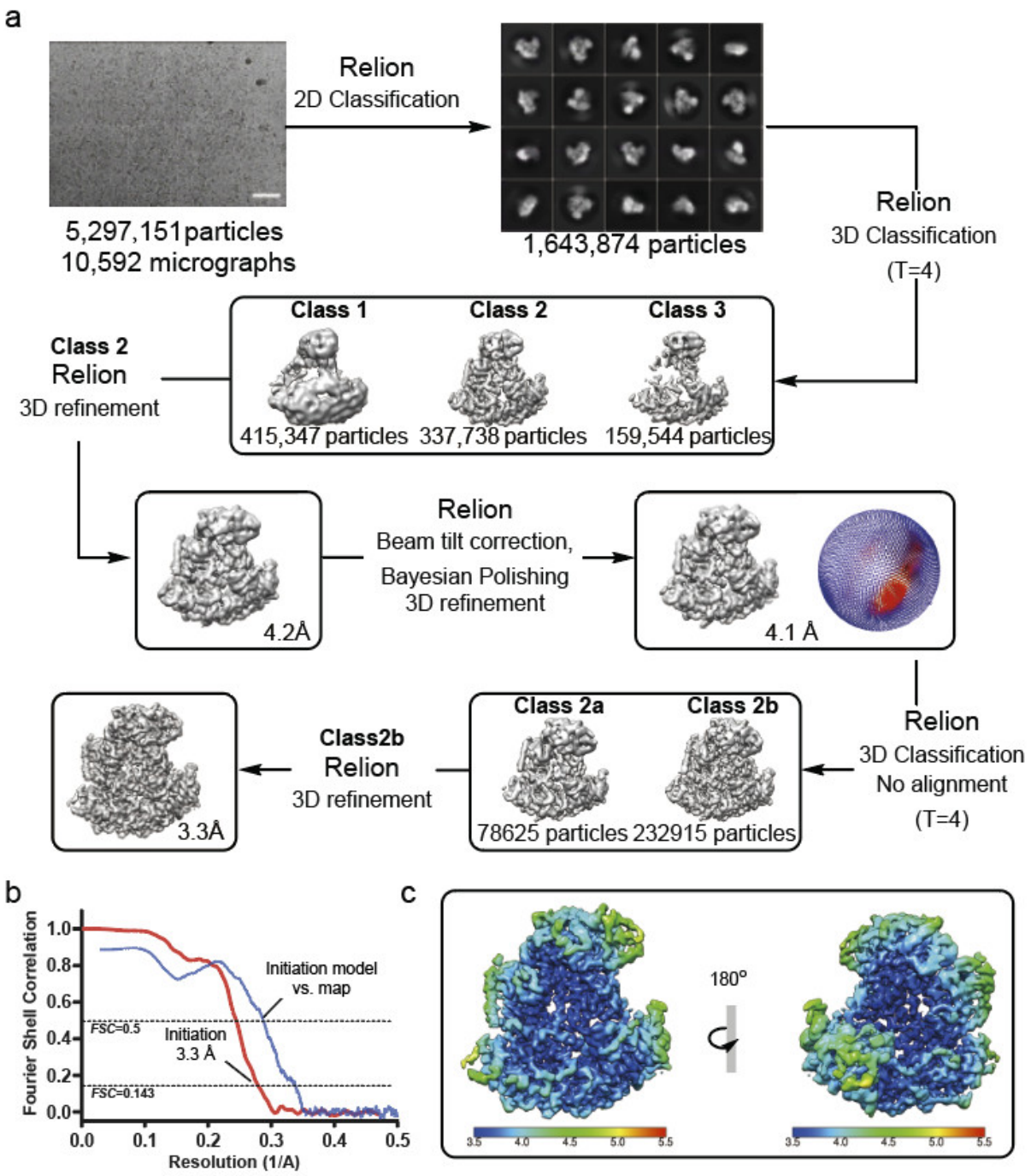

374

375

376 **Fig. S3: Single-particle cryo-EM analyses of the Ubr1-Ubc2-Ub-Degron dataset.**

a, The workflow of data processing. The dataset was subjected to particle selection, 2D classification, and multiple rounds of 3D classification. A representative micrograph (scale bar corresponds to 50 nm) and representative 2D class averages are shown. The distribution of the Euler angles is shown next to the map. **b,** Fourier shell correlation (FSC) curve of the masked map after Relion postprocessing. The resolution was determined by the FSC=0.143 criterion. The model vs. map FSC curve is also shown. **c,** Local resolution of the map calculated using Relion.

385 **FIG. S4**

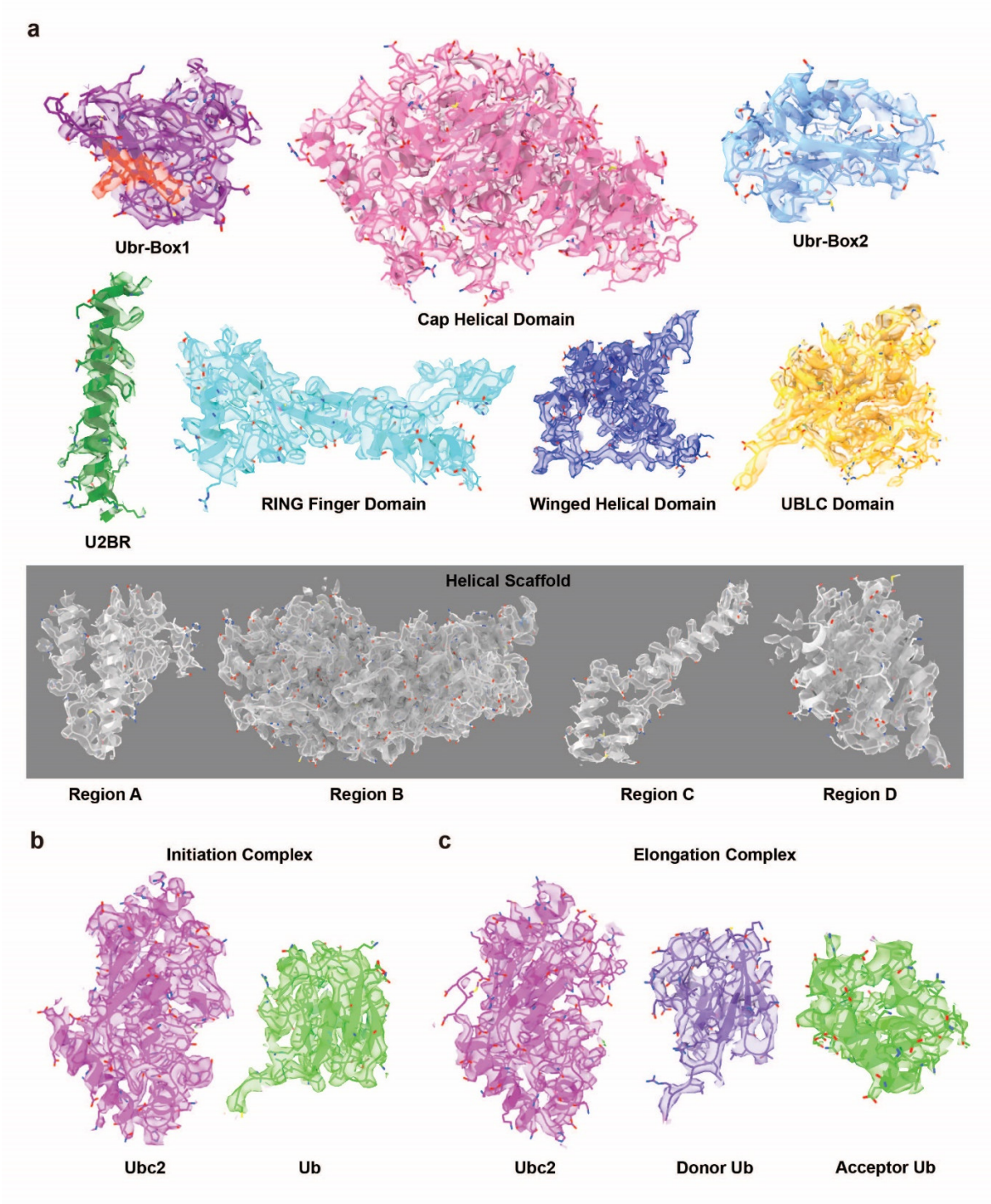

386

387

388

389 **Fig. S4: Representative cryo-EM densities of the initiation and elongation complexes.**

390 **a**, Individual domains in the initiation complex. **b**, Ubc2 and Ub in the initiation complex. **c**,
391 Ubc2, donor Ub and acceptor Ub in the elongation complex. Maps in panels **a** and **b** were
392 sharpened using a B factor of -96.5 $Å^2$ and contoured at a level of 0.03. Maps in panel **c** were
393 sharpened using a B factor of -96.7 $Å^2$ and contoured at a level of 0.022.

394

FIG. S5

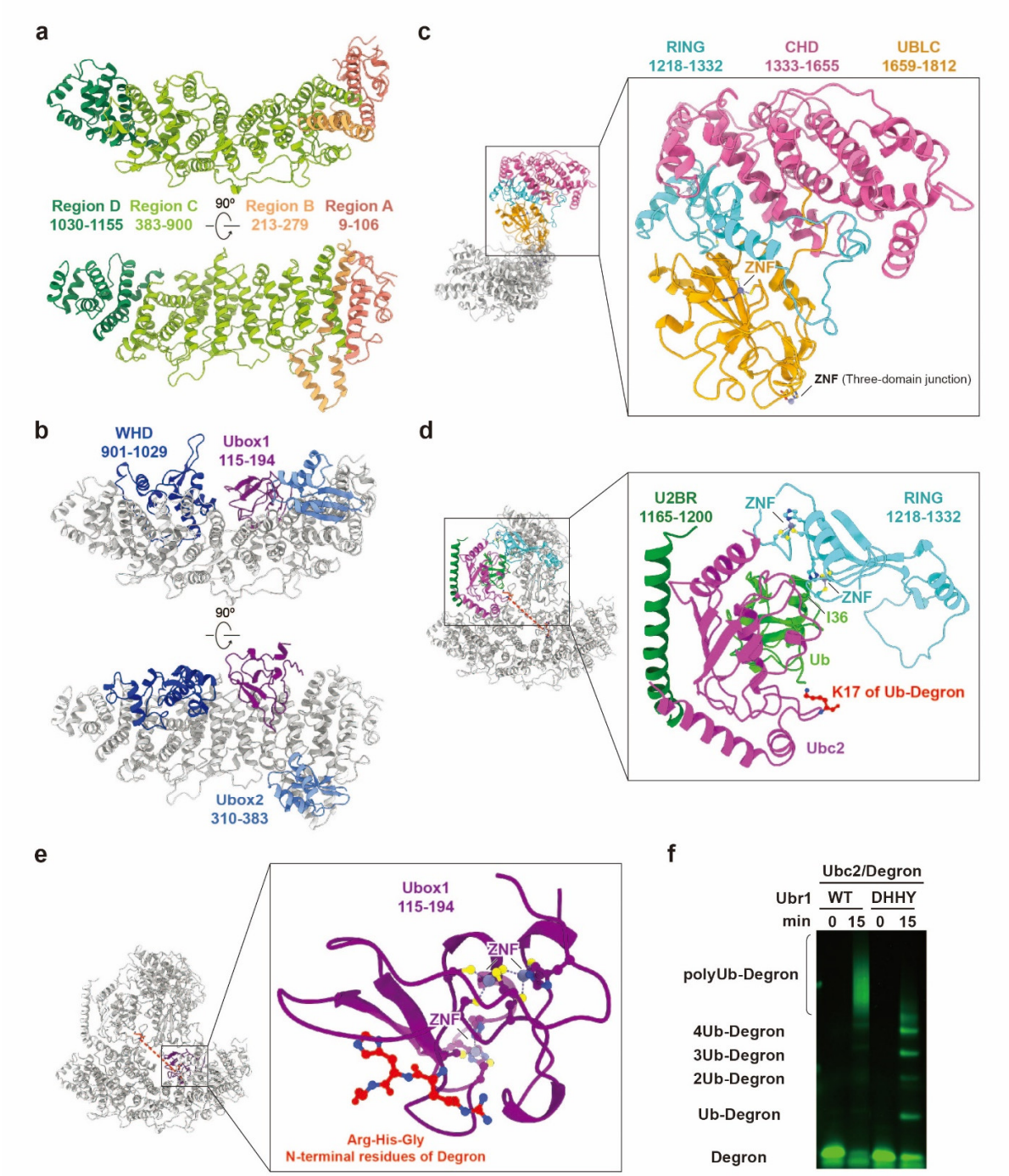
a
Region D
1030-1155
Region C
383-900
90°
Region B
213-279
Region A
9-106
b
WHD
901-1029
Ubox1
115-194
90°
Ubox2
310-383
c
RING
1218-1332
CHD
1333-1655
UBLC
1659-1812
ZNF
ZNF (Three-domain junction)
d
U2BR
1165-1200
ZNF
RING
1218-1332
ZNF
I36
Ub
K17 of Ub-Degron
Ubc2
e
Ubox1
115-194
ZNF
ZNF
Arg-His-Gly
N-terminal residues of Degron
f
Ubc2/Degron
Ubr1
WT
DHHY
min
0
15
0
15
polyUb-Degron
4Ub-Degron
3Ub-Degron
2Ub-Degron
Ub-Degron
Degron

399 **Fig. S5: Molecular structures of Ubr1 domains.**

400 **a,** The helical scaffold of Ubr1 consists of four separate regions. **b,** The three domains located
401 around the helical scaffold, Ubr-Box1 (Ubox1, purple), Ubr-Box2 (Ubox2, light blue) and winged
402 helical domain (WHD, dark blue). **c,** The three domains above the helical scaffold, the RING
403 finger domain (cyan), cap helical domain (pink) and UBLC domain (yellow). The RING finger
404 domain joins the cap helical domain and UBLC domain. An additional zinc finger motif (ZNF) in
405 UBLC is labelled. **d,** The U2BR (forest green), Ubc2 (magenta)~Ub (lime) and the RING finger
406 domain form the catalytic module of Ubr1. Two zinc finger motifs (ZNF) in the RING finger
407 domain are labelled. **e,** A close-up view of substrate-engaged Ubr-Box1. Three zinc finger
408 motifs (ZNF) are labelled. **f,** In vitro Ubr1-dependent ubiquitination assay. A quadruple mutant
409 (H161A, Y933A, D1175A, and H1763A) of the residues involved in the interface between
410 Ubox1, WHD, and UBLC (three-domain junction, shown in **Fig. 1f**) was tested.

411

412 **FIG. S6**

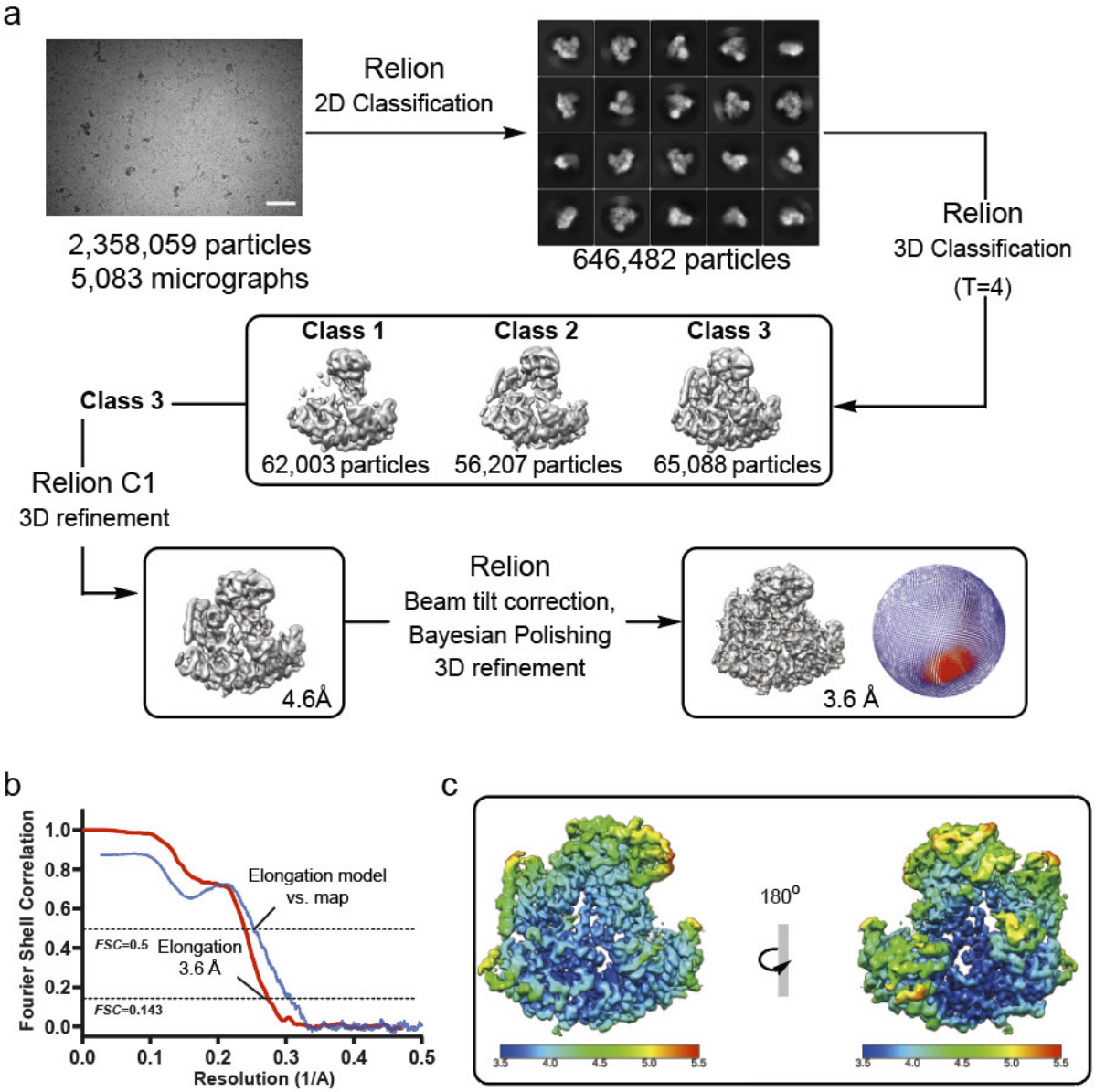

413

414

415

416

417 **Fig. S6: Single-particle cryo-EM analyses of the Ubr1-Ubc2-Ub-Ub-Degron dataset.**

a, The workflow of data processing. The dataset was subjected to particle selection, 2D classification, and multiple rounds of 3D classification. A representative micrograph (scale bar corresponds to 50 nm) and representative 2D class averages are shown. The distribution of the Euler angles is shown next to the map. **b,** Fourier shell correlation (FSC) curve of the masked map after Relion postprocessing. The resolution was determined by the FSC=0.143 criterion. The model vs. map FSC curve is also shown. **C,** Local resolution of the map calculated using Relion.

426 **FIG. S7**

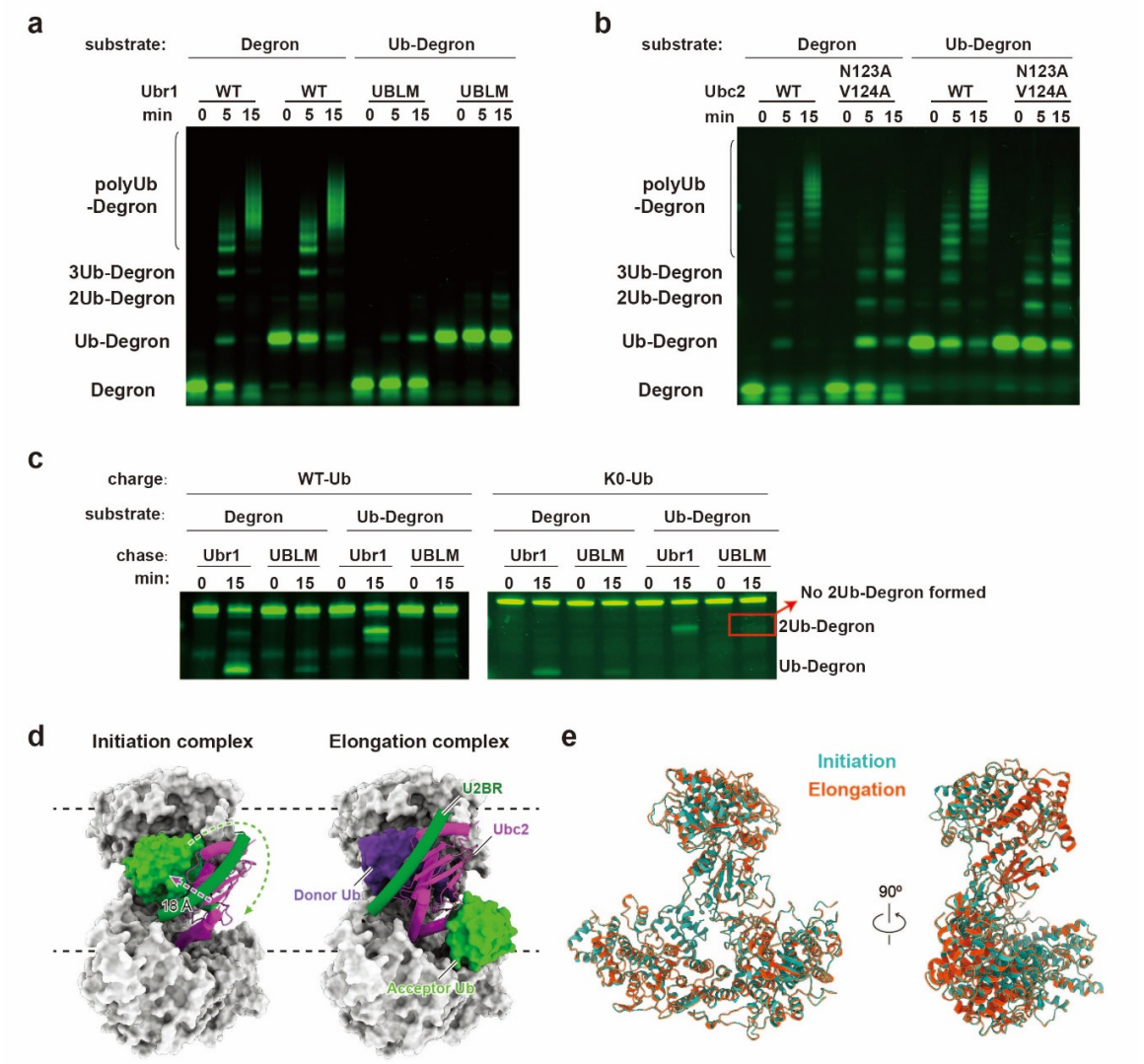

427

428

429 **Fig. S7: Characterization of the acceptor Ub interactions in the elongation complex.**

430 **a-b**, In vitro Ubr1-dependent ubiquitination assays. Mutations of the Ub binding loop
431 (H678A/V679A/L680A/H681A, UBLM, panel **a**) and the Ubc2 interface (N123A/V124A, panel **b**)
432 were tested. **c**, Single-turnover ubiquitination assay of wild-type Ubr1 and the Ubr1 mutant
433 (UBLM) using Ubc2 charged with either wild-type Ub or K0-Ub (all lysines mutated to arginines).
434 The red box highlights that the Ubr1 mutant (UBLM) could not mediate Ub thioester discharge
435 from Ubc2~Ub to Ub-degron (a defect in elongation). **d**, Side views of the initiation and
436 elongation complexes showing the displacement of U2BR, Ubc2, and Ub. **e**, Alignment of Ubr1
437 in the initiation and elongation complexes.

438

439 **FIG. S8**

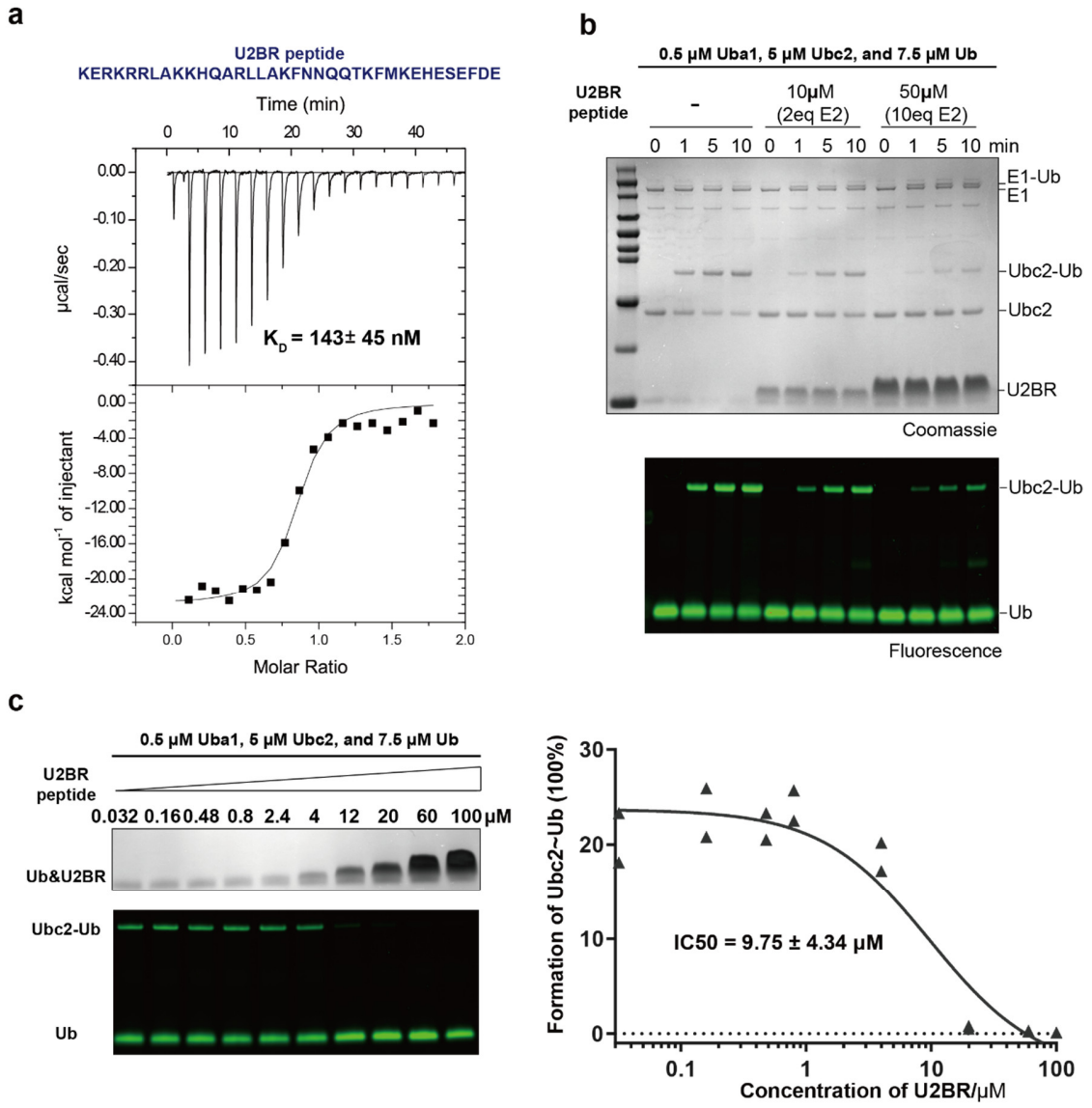

440

441 **Fig. S8: Characterization of the U2BR peptide on the enzymatic properties of Ubc2.**

442 **a**, ITC measurement of the binding between Ubc2 and a synthetic U2BR peptide. **b**, E1-

443 dependent Ubc2~Ub thioester formation in the presence of the synthetic U2BR peptide. **c**,

444 Quantitative evaluation of the inhibitory effects of the synthetic U2BR peptide on E1-dependent

445 Ubc2~Ub thioester formation. Averages of two independent experiments were plotted and fit to

446 estimate the IC50 of the synthetic U2BR peptide.

447

448 **FIG. S9**

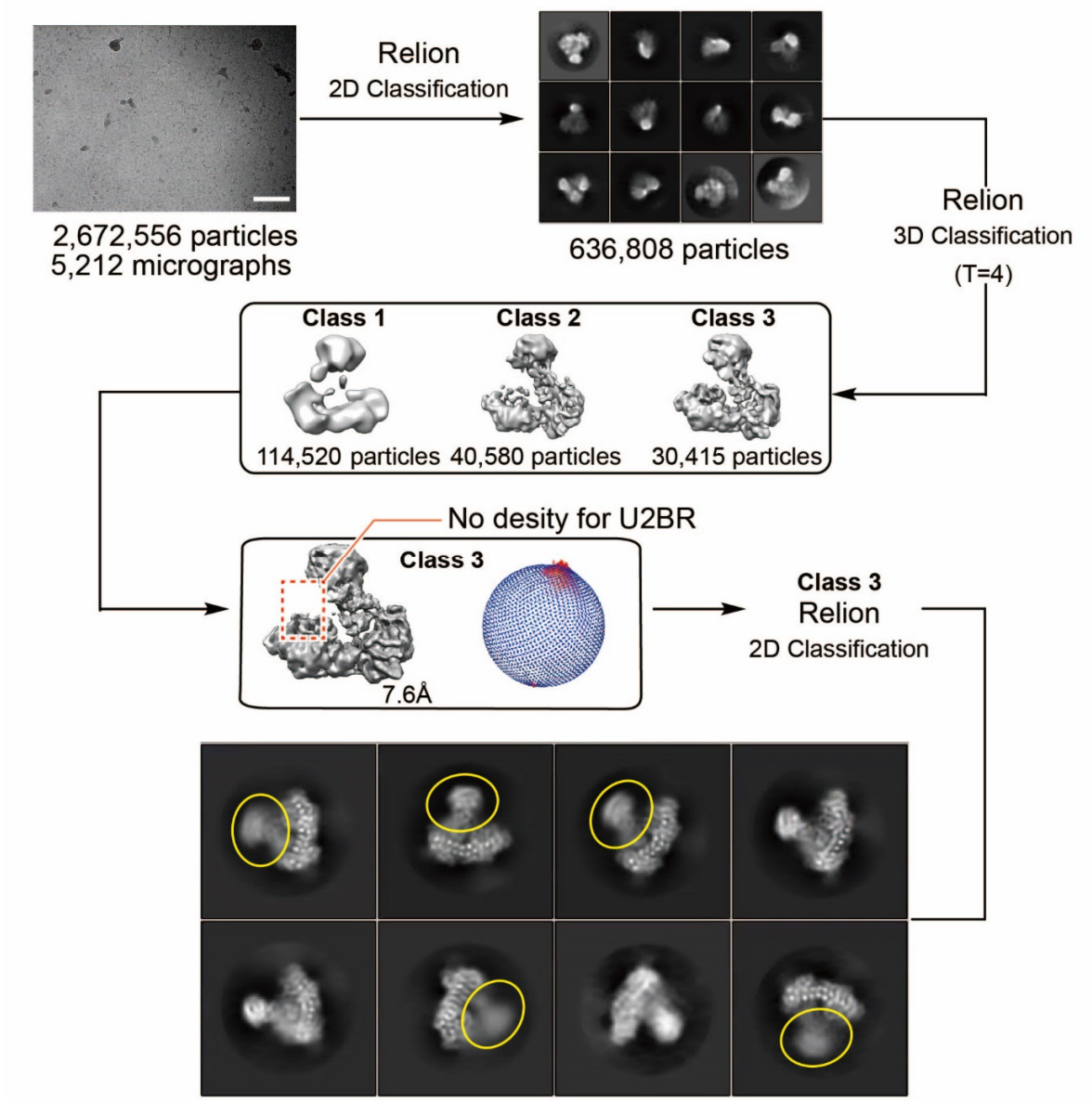

449

450

451

452 **Fig. S9: Single-particle cryo-EM analyses of Ubr1.**

453 The dataset was subjected to particle selection, 2D classification, and multiple rounds of 3D
454 classification. A representative micrograph (scale bar corresponds to 50 nm) and representative
455 2D class averages are shown. Flexible cap helical domains in the 2D class averages are
456 highlighted in yellow circles. The distribution of the Euler angles is shown next to the map.

457

458 **Table S1: Statistics of cryo-EM data collection and processing**

	Initiation complex	**Elongation complex**	**Apo Ubr1**
Detergent	FOM (0.001%)	FOM (0.001%)	FOM (0.001%)
Microscope	Krios (UChicago)	Krios (UChicago)	Krios (NCI)
Magnification	81,000	81,000	81,000
Voltage (kV)	300	300	300
Spherical aberration (mm)	2.7	2.7	2.7
Detector	K3	K3	K3
Camera mode	Super resolution counting	Super resolution counting	Super resolution counting
Exposure rate (e^-/pixel/s)	15	15	15
Total exposure (e^-/Å^2)	50	50	50
Defocus range (μm)	-1.0 to -2.5	-1.0 to -2.5	-1.0 to -2.5
Pixel size (Å)	1.063	1.063	1.122
Mode of data collection	Image shift	Image shift	Image shift
Energy filter	20 eV slit	20 eV slit	20 eV slit
Software for data collection	EPU	EPU	Latitude S
Number of micrographs	10,592	5,083	5,212
Symmetry imposed	C1	C1	C1
Box size (pixel)	320	320	320
Initial particle images (no.)	5,297,151	2,358,059	2,672,556
Particle images for 3D (no.)	1,643,874	646,482	636,808
Final particle images (no.)	232,915	65,088	30,415
Map resolution, masked (Å)	3.35	3.67	4.56
B-factor estimated (Å^2)	96.5	96.7	119.0
EMD accession code	23806	23807	-

459

460

461 **Table S2: Statistics of cryo-EM model refinement and geometry**

	Initiation complex	**Elongation complex**
Composition (#)		
Chains	5	7
Atoms	15934	16488
Residues	1967	2036
Water	0	0
Ligands	ZN: 7	ZN: 7
		ETE: 1 (chemical linker)
Bonds (RMSD)		
Length (Å)	0.003	0.004
Angles (°)	0.604	0.646
MolProbity score	1.74	1.77
Clash score	10.39	11.19
Ramachandran plot (%)		
Outliers	0.00	0.00
Allowed	3.29	3.27
Favored	96.71	96.73
Rotamer outliers (%)	0.28	0.27
Cβ outliers (%)	0.00	0.00
Peptide plane (%)		
Cis proline/general	0.0/0.0	0.0/0.0
Twisted proline/general	0.0/0.0	0.0/0.0
CaBLAM outliers (%)	1.81	1.5
ADP (B-factors)		
Iso/Aniso (#)	15934/0	16488/0
min/max/mean		
Protein	12.90/108.84/44.62	30.00/164.26/82.92
Ligand	53.14/105.95/73.23	94.39/153.23/112.90
PDB accession code	7MEX	7MEY

462

463

464

465 **METHODS**

466 **Cloning and plasmid construction**

467 The plasmid containing yeast (*Saccharomyces cerevisiae*) Ubr1 was purchased from Addgene
468 (plasmid # 24506) [41]. DNA sequence of yeast (*Saccharomyces cerevisiae*) Ubc2 was
469 synthesized and codon optimized for *E. coli* overexpression by Genscript. The gene was further
470 cloned between the NdeI and XhoI sites of the vector pET-28a containing an N-terminal His tag
471 followed by a HRV3C protease cleavage site. Variants of Ubr1 and Ubc2 were generated using
472 site directed mutagenesis. Human Uba1 was cloned in pET-28a vector containing an N-terminal
473 His tag. DNA sequences of wildtype ubiquitin (Ub), Ub mutants including K48R, G76C, K0 (all 7
474 lysine residues mutated to arginine), and AC-Ub (a Ub variant with additional two amino acids
475 Ala-Cys at the N terminus) were synthesized and codon optimized for *E. coli* overexpression by
476 Genscript. The genes were further cloned between the NdeI and XhoI sites of the vector pET-
477 22b.

478

479 **Protein expression and purification**

480 Wildtype Ub and Ub mutants were purified as previously described [42]. Briefly, plasmids for
481 overexpression were transformed to *E. coli* BL21(DE3) competent cells. The *E. coli* cells were
482 grown in Luria broth (LB) media containing 50 µg/mL ampicillin until OD600 reached 0.8 and
483 were induced by isopropyl β-D-1-thiogalactopyranoside (IPTG) at a final concentration of 0.4
484 mM followed by overnight incubation at 25 °C. Cells were pelleted at 4,000 rpm for 30 min at
485 4 °C, resuspended in ddH2O and lysed by ultra-sonication for 30 min in an ice bath. The cell
486 lysates were supplemented with 1% perchloric acid to precipitate non-relevant proteins which
487 were then cleared using centrifugation (30 min, 15,000×g, 4 °C). Ub and its variants were
488 further purified using a Mono S cation exchange column (GE Healthcare), followed by dialysis
489 into a buffer containing 50 mM HEPES, pH 7.5, and 150mM NaCl. The peak fractions were
490 pooled and concentrated to 20 mg/ml.

491 Plasmids containing Ubc2 and its variants were transformed to *E. coli* BL21(DE3) competent
492 cells. The *E. coli* cells were grown in LB media containing 20 µg/mL kanamycin until OD600

493 reached 0.6, and were induced by IPTG at a final concentration of 0.4 mM followed by overnight
494 incubation at 18 °C. Cells were harvested by centrifugation at 4,000 rpm for 30 min and then
495 lysed by sonication in the lysis buffer (50 mM HEPES, pH 7.5, 150mM NaCl, 20mM imidazole
496 and 1mM PMSF). After centrifugation at 12,000 rpm for 30 min, the supernatant was loaded
497 onto a Ni-NTA affinity column. The proteins were eluted with the elution buffer (50 mM HEPES,
498 pH 7.5, 150mM NaCl, and 400mM imidazole), and further purified by a Superdex 200 size-
499 exclusion column (GE Healthcare) equilibrated in a buffer containing 50 mM HEPES, pH 7.5,
500 and 150 mM NaCl.

501 Yeast Ubr1 and its variants was expressed as previously described [33]. Briefly, single colony of
502 yeast were grown in SD medium at 30°C until OD600 reached ~1.0. The cells were pelleted at
503 5,000 g, washed once with cold phosphate buffer saline (PBS), and then resuspended (6 mL
504 buffer per 1 g of pellet) in the lysis buffer (50 mM HEPES, pH 7.5, 0.15 M NaCl, protease
505 inhibitor cocktail (Roche), 1mM PMSF, and 10% glycerol,). The resuspended yeast cells were
506 dropped into liquid nitrogen, and the frozen pellet balls were ground to fine powder in liquid
507 nitrogen using a cryogenic impact grinder (SPEX™ SamplePrep 6870 Freezer/Mill). The powder
508 was further thawed and centrifuged at 11,200 g at 4°C for 30 min. The supernatant was loaded
509 onto anti-DYKDDDDK (FLAG) affinity resin (Thermo Scientific, #. A36803), followed by
510 extensive wash. Finally, the FLAG-tagged Ubr1 was eluted with 1mg/mL FLAG peptide and
511 further purified by a Superose 6 size-exclusion column (GE Healthcare) equilibrated in a buffer
512 captaining 50 mM HEPES, pH 7.5, and 150mM NaCl.

513

514 **Peptide Synthesis**

515 All peptides were synthesized using standard Fmoc solid phase peptide synthesis (SPPS)
516 protocols under standard microwave conditions (CEM Liberty Blue). Fmoc-hydrazine 2-
517 chlorotrityl chloride PS resin and Rink Amide MBHA PS resin were used for peptides synthesis.
518 The coupling cycle was programed as previously reported [18]. Briefly, 10% piperidine in DMF
519 with 0.1 M Oxyma (1 min at 90 °C) was applied as deprotection condition, and 4-fold of 0.2 M
520 Fmoc-protected amino acid, 1.0 M DIC, and 1.0 M Oxyma in DMF (10 min at 50 °C for His and

521 Cys, 90 °C for other residues were applied as amino acid coupling condition. Specifically, in
522 peptide Ub(46-76)-^{K17}Degron-NH_2 and Ub(48-76)-^{K17}Degron-NH_2, Fmoc-Lys (Alloc)-OH was
523 coupled at position 17 for the orthogonal protection. When the backbone coupling was finished,
524 the Alloc protecting group was removed by $[(Ph_3)P]_4Pd/Ph_3SiH$ as previously described [43], and
525 then the ε-amino group on Lys17 can be further coupled with successive sequence (Ub48-76)
526 or (Ub46-76). After the completion of SPPS, the resulting peptide-resin was cleaved in cleavage
527 cocktail (87% trifluoroacetic acid, 5% water, 5% thioanisole, 3% 1,2-ethanedithiol) for 2 h at
528 25 °C. Crude peptides were precipitated with cold diethyl ether, analyzed and purified by
529 reversed-phase high-performance liquid chromatography (RP-HPLC).
530

531 **Preparation of fluorescence labeled Degron and Ub-Degron**

532 Degron was direct obtained from SPPS as described above. K17-linked mono ubiquitinated
533 degron (Ub-^{K17}Degron) was synthesized from two fragments, Ub(1-45)-$NHNH_2$ and Ub(46-76)-
534 ^{K17}Degron-NH_2. Ala46 in the latter fragment was temporally mutated to Cys to enable native
535 chemical ligation of these two fragments. After ligation the thiol group of Cys46 was removed
536 through desulfurization reaction to produce the native Ala46 as shown in Fig S1b. For
537 fluorescence labeling of Degron, we introduced an additional Cys at the C-terminus of Degron to
538 enable site-specific labeling. In the Ub-Degron case, a Cys(Acm) was introduced in the C-
539 terminus of Degron to orthogonally protect this thiol group from being desulfurized. After
540 purification, the Acm group was removed from the obtained Ub-Degron-Cys(Acm) to free the
541 thiol group for labeling. For labeling reaction, 2 mg lyophilized dry power of Degron-Cys or Ub-
542 Degron-Cys was dissolved in 50 mM HEPES, 150mM NaCl, pH 7.5. Then 2 equivalents of
543 fluorescein-5-maleimide (Invitrogen, #F150) was added and the mixture was incubated at room
544 temperature for 20 min, followed by buffer exchange in (50 mM HEPES, 150mM NaCl, pH 7.5)
545 using a Superdex peptide size-exclusion column (GE Healthcare) to give the fluorescence
546 labeled degron and Ub-degron.
547

548 **Ubiquitination assay with fluorescent Degron or Ub-Degron**

549 In vitro ubiquitination assays were performed with 0.1 μM Uba1, 4 μM Ubc2, 0.25 μM Ubr1, 5
550 μM fluorescent Degron or Ub-Degron, and 80 μM Ub at 30 °C in the reaction buffer (50 mM
551 HEPES pH 7.5, 0.15 M NaCl, 10 mM $MgCl_2$, and 5 mM ATP). The reactions were terminated by
552 adding 4 × SDS-sample buffer, followed by SDS-PAGE. Unless indicated otherwise, same
553 concentrations of Ubr1 and Ubc2 variants as the respective wildtype were used in the assay.
554

555 **Single-turnover measurement of Ub transfer in the initiation and elongation steps**

556 To monitor the single-turnover of Ub transfer in the initiation step, i.e., Ubr1 transfers Ubc2~Ub
557 to Degron, a pulse-chase experiment that eliminates the effects of UBA1-dependent formation
558 of Ubc2~Ub intermediate was performed. The pulse reaction generated a thioester-linked
559 Ubc2~Ub intermediate with 5 μM Ubc2, 7.5 μM fluorescent Ub, 0.5 μM UBA1 in a buffer
560 containing 50 mM HEPES pH 8.0, 150 mM NaCl, 10 mM $MgCl_2$, and 10 mM ATP. The reaction
561 mixture was incubated at room temperature for 10 min, and quenched with 50 mM EDTA on ice
562 for 5 min. A final concentration of 0.5 μM Ubr1 and 25 μM fluorescently labeled Degron was
563 added for the chase reaction which was then incubated at 30°C for 5 minutes. The reaction was
564 stopped by in 2× SDS-sample buffer (pH < 3), followed by SDS-PAGE. Same concentrations of
565 Ubr1 and Ubc2 variants as the respective wildtype were used. The experimental setup for the
566 elongation step was similar to the initiation step, except that fluorescently labeled Ub-Degron
567 was used instead of Degron.
568

569 **Michaelis-Menten constant (Km) measurement of the initiation and elongation steps**

570 For K_m measurement of the initiation step, two prepared mixtures are required. Mixture 1
571 consists of Uba1 and Ub (K48R), and Mixture 2 consists of Ubr1 and fluorescently labelled
572 Degron. Both mitures were prepared in the reaction buffer (50 mM HEPES pH 7.5, 150 mM
573 NaCl, 10 mM $MgCl_2$, and 5 mM ATP). Ubc2 was prepared as a twofold dilution series from the
574 stock, and then introduced into the solution containing equal amounts of the 2 mixtures to
575 initiate the reaction. The final concentrations were 80 μM Ub (K48R), 0.1 μM Uba1, 0.25 μM
576 Ubr1 and 5 μM fluorescently labelled Degron. Reactions were quenched after 1 minute at 30°C

using 2 × SDS-sample buffer, followed by SDS-PAGE. The gels were imaged on ChemiDoc MP Imaging System. Substrate and product bands were individually quantified as a percentage of the total signal for each time point using ImageLab (Bio-Rad). Ratios of ubiquitinated products relative to the total signal were plotted against the concentration of Ubc2 and fit to the Michaelis–Menten equation to estimate K_m in GraphPad Prism 8. The experimental setup for K_m measurement of the elongation step was similar, except that fluorescently labeled Ub-Degron was used instead of Degron.

Generation of the stable complex mimicking the transition state of the initiation step

1. Preparation of Ub(1-75) hydrazide

Ub(1-75) hydrazide (Ub75-$NHNH_2$) were generated using previously reported protein hydrazinolysis method [42]. In brief, Ub(G76C) of which Gly76 at the C-terminus was mutated to Cys could undergo N-S acyl transfer so that hydrazine could be used as a suitable nucleophile, leading to a reliable C-terminal hydrazinolysis. 20 mg/mL Ub(G76C), 5 mg/mL TCEP, 50 mg/mL $NHNH_2$•HCl, and 100 mg/mL MesNa were mixed in 20 mM Tris, pH 6.5, and stirred at 60 rpm and 50°C for 24 hours. The final products were purified and analyzed by RP-HPLC.

2. Preparation of Ub(G76C)-^{K17}Degron

The reaction scheme was shown in Extended Data Fig. 3a. In brief, Ub75-$NHNH_2$ peptide (1 μmol, 1 equiv) was dissolved in 1mL ligation buffer (6 M guanidinium chloride, 100 mM NaH_2PO_4, pH 2.3) precooled to -15 °C. Then 10 μL 1 M $NaNO_2$ (10 μmol, 10 equiv) was added, and the reaction was stirred for 30 min at -15 °C to fully convert the hydrazide to the acyl azide. Next, sodium 2-mercaptoethanesulfonate (MesNa, 100 μmol, 100 equiv) was added, and the pH was adjusted to 5.0 for overnight reaction. The product, Ub75-MesNa, was further purified by RP-HPLC. Purified Ub1-75-MesNa (1 μmol, 1 equiv) and Cys-^{K17}Degron peptide (1.1 μmol, 1.1 equiv) were mixed to the ligation buffer (6 M guanidinium chloride, 100 mM NaH_2PO_4, 5mg/mL TCEP, pH 7.4). Next, 4-mercaptophenylacetic acid (MPAA, 50 μmol, 50 equiv) was added, and

603 the pH was adjusted to 6.4 for overnight reaction. The final product, Ub(G76C)-^{K17}Degron, was
604 purified and analyzed by RP-HPLC.

605 **3. Preparation of Ubc2-Ub(G76C)-^{K17}Degron through disulfide ligation**

606 Lyophilized dry power of Ub(G76C)-^{K17}Degron (1.3 mg) was dissolved in 100 μL 6 M
607 guanidinium chloride, 50 mM HEPES, pH 7.5 to a final concentration of 1mM. 2 μL of 100 mM
608 5,5′ -dithiobis-(2-nitrobenzoic acid) (Sigma Aldrich, dissolved in 50 mM NaH_2PO_4, pH 7.5) was
609 immediately added and fully mixed by pipetting before incubating at room temperature for 20
610 min. The solution was then diluted to the refolding buffer containing 50 mM HEPES pH7.5,
611 150mM NaCl. Excess reactants were removed by a Superdex peptide size-exclusion column
612 (GE Healthcare) equilibrated in the refolding buffer. Finally, the product and 0.9 equiv Ubc2
613 (pre-dialyzed into the refolding buffer) were mixed and incubated at room temperature for 30
614 min. The final product was purified and analyzed by RP-HPLC.
615

616 **Generation of the stable complex mimicking the transition state of the elongation step**

617 **1. Preparation of Molecule 2**

618 As shown in Fig. 2b, **Molecule 2** was prepared using Cys-aminoethylation reaction[36].
619 Specifically, 1 μmol lyophilized powder of Ubc2 was incubated in aqueous alkylation buffer (6 M
620 guanidinium chloride, 0.1 M HEPES pH 8.5, 5 mg/mL TCEP) with 40 mM **Molecule 1** (2-((2-
621 chloroethyl)amino)ethane-1-(S-acetaminomethyl)thiol) at 37 °C for 14-16 h. The product,
622 **Molecule 2**, was further purified by semi-preparative HPLC and lyophilized.

623 **2. Preparation of Molecule 3**

624 Lyophilized **Molecule 2** was dissolved in reaction buffer containing 6 M guanidinium chloride,
625 0.1 M NaH_2PO_4 buffer, pH 7.4 at a final concentration of 1 mM. Then $PdCl_2$ (15 equiv, pre-
626 dissolved in the reaction buffer) was added and the mixture was incubated at 37°C for 1 h to
627 remove the Acm group. Purified Ub(1-75)-MesNa (1 μmol, 1 equiv) and Molecule 2 (1.1 μmol,
628 1.1 equiv) were then mixed in the ligation buffer (6 M guanidinium chloride, 100 mM NaH_2PO_4,
629 5mg/ml TCEP, pH 7.4). Next, 4-mercaptophenylacetic acid (MPAA, 50 μmol, 50 equiv) was

630 added, and the pH was adjusted to 6.4 to initiate native chemical ligation. The product was
631 purified and analyzed by RP-HPLC.

632 **3. Preparation of Ub^{K48C}-^{K17}Degron**

633 Different from the preparation strategy for Ub-Degron, we mutated the Lys48 to Cys, which
634 enabled native chemical ligation. Furthermore, the thiol group on Cys48 was retained for
635 disulfide ligation. Specifically, Ub(1-47)$NHNH_2$ peptide (1 μmol, 1 equiv) was dissolved in 1mL
636 ligation buffer (6 M guanidinium chloride, 100 mM NaH_2PO_4, pH 2.3) precooled to -15 °C. Then,
637 10 μL 1 M $NaNO_2$ (10 μmol, 10 equiv) was added, and the reaction was stirred for 30 min at -
638 15 °C to fully convert the hydrazide to acyl azide. Next, Ub(48-76)^{K48C}-^{K17}Degron peptide (1.1
639 μmol, 1.1 equiv) was added to the ligation buffer, followed by 4-mercaptophenylacetic acid
640 (MPAA, 50 μmol, 50 equiv). The pH was adjusted to 6.4 to initiate the ligation. The product,
641 Ub^{K48C}-^{K17}Degron, was purified and analyzed by RP-HPLC.

642 **4. Preparation of Ubc2-Ub-Ub^{K48C}-^{K17}Degron using disulfide ligation**

643 Lyophilized dry power of **Molecular 3** was dissolved in 500ul 6 M guanidinium chloride, 50mM
644 HEPES, 1mM TCEP, pH7.5, and refolded through gradient dialysis against refolding buffer
645 (50mM HEPES, 1mM TCEP, pH7.5) containing 6M, 2M, 1M to 0M guanidinium chloride. 1.3mg
646 Lyophilized dry power of **Ub^{K48C}-^{K17}Degron** was dissolved in 100 μl 6 M guanidinium chloride,
647 50mM HEPES, pH7.5 (the final concentration was 1mM), and then 2μl 100mM 5,5′ -dithiobis-
648 (2-nitrobenzoic acid) (Sigma Aldrich, dissolved in 50 mM NaH_2PO_4 pH 7.5) was added and fully
649 mixed by pipetting before incubating at room temperature for 20 min. The solution was then
650 diluted to the refolding buffer, and the excess small molecular was removed by Superdex
651 peptide size-exclusion column (GE Healthcare) equilibrated in refolding buffer. Finally, the
652 pooled product and 1.1eq refolded **Molecular 3** were mixed and incubated at room temperature
653 for 30 min. The final product, **Ubc2-Ub-Ub^{K48C}-^{K17}Degron**, was purified and analyzed by RP-
654 HPLC.
655

656 **Specimen preparation for single-particle cryo-EM**

657 Ubr1 (0.4 mg/mL) was mixed with 1.5-fold excess (molar ratio) initiation or elongation
658 intermediate-mimics and incubated on ice for 30 min. A final concentration of 0.01% fluorinated
659 octyl maltoside (FOM) was immediately added to the sample before grid freezing using a
660 Vitrobot mark IV (Thermo Fisher) operating at 8 °C and 100% humidity. A volume of 3.5 µL
661 sample was applied to a glow-discharged Quantifoil Cu 1.2/1.3 grid, and blotted for 1 second
662 using standard Vitrobot filter paper (Ted Pella, 47000-100) before plunge freezing in liquid
663 ethane.
664

665 **Data collection for single-particle cryo-EM**

666 Optimized frozen grids were sent to Advanced Electron Microscopy Facility at the University of
667 Chicago or National Cryo-Electron Microscopy Facility at National Cancer Institute for data
668 collection. All datasets were acquired as movie stacks with a Titan Krios electron microscope
669 (Thermo Scientific) operating at 300 kV, equipped with a Gatan K3 direct detection camera. A
670 single stack consists of 40 frames with a total exposure around 50 electrons/Å^2. The defocus
671 range was set at -1.0 to -2.5 µm. See **Table S1** for the details.
672

673 **Image processing**

674 Movie stacks were subjected to motion correction using MotionCor2 [44]. CTF parameters for
675 each micrograph were determined by CTFFIND4 [45]. The following particle picking, two- and
676 three-dimensional classifications, and three-dimensional refinement were performed in RELION-
677 3 [23]. About 2,000 particles were manually picked to generate 2D class averages. The class
678 averages were then used as templates for the following automatic particle picking. False-
679 positive particles or particles classified in poorly defined classes were discarded after 2D
680 classification. Initial 3D classification was performed on a binned dataset using the initial model
681 obtained in RELION. The detailed data processing flows are shown in Extended Data Figs. 3
682 and 5. Data processing statistics are summarized in **Table S1**. Reported resolutions are based

683 on Fourier shell correlation (FSC) using the FSC=0.143 criterion. Local resolution was
684 determined using the implementation in RELION.
685

686 **Model Building, Refinement, and Validation**

687 Ubr1 is a single-subunit E3 with more than 1,900 amino acids. Only was the structure of Ubr-
688 Box1 domain determined previously [24]. To overcome the difficulty during model building, we
689 used artificial intelligence (AI) based de novo modelling tool DeepTracer program [25] to build a
690 starting model of the entire complex from scratch. Specifically, the sharpened map of the
691 initiation complex and a FASTA file containing sequences of Ubr1, Ubc2, and Ub were input to
692 the online server of DeepTracer (https://deeptracer.uw.edu/home). The program finished within
693 10 minutes and output a complete model with Ubc2, and Ub correctly positioned. About 80% of
694 Ubr1 was also correctly built into the cryo-EM map, with some errors in the poorly resolved
695 regions and the zinc-binding sites. The starting model was first refined in real space using
696 PHENIX [27], and then manually fixed, adjusted and refined using COOT [26]. At the end, about
697 1800 residues of Ubr1 were built. The registration of the main chain was carefully checked and
698 fixed based on bulky residues. The entire procedure was greatly simplified and accelerated with
699 the starting model from DeepTracer. The final model was refined again in real space using
700 PHENIX [27]. The statistics of model refinement and geometry is shown in **Table S2**. Molecular
701 graphics and analyses were performed with UCSF ChimeraX[46] and 'Protein interfaces, surfaces
702 and assemblies' service PISA at the European Bioinformatics Institute.
703 (http://www.ebi.ac.uk/pdbe/prot_int/pistart.html) [47].

704

705 **Ubc2~Ub thioester formation in the presence of U2BR peptide**

706 First, 0.5 μM Uba1, 5 μM Ubc2, and 7.5 μM fluorescently labeled Ub was mixed in the reaction
707 buffer containing 50 mM HEPES pH 8.0, and 150 mM NaCl. U2BR peptide was prepared as a

708 twofold dilution series from the stock and added to the reaction mixture. Prepared ATP·Mg^{2+}
709 mixture (50 mM $MgCl_2$, 50 mM ATP, pH 8.0) was added to initiate the Ubc2~Ub thioester
710 formation. Reactions were quenched after 1 minute at 30 °C using 2 × SDS-sample buffer (pH <
711 3), followed by SDS-PAGE. The gels were imaged on ChemiDoc MP Imaging System, and
712 substrate and product bands were quantified respectively as a percentage of the total signal for
713 each time point using ImageLab (Bio-Rad). Ratio of ubiquitylated products relative to the total
714 signal was plotted against the concentrations of Ubc2 and fit to the inhibitor vs. response model
715 (three parameters) in GraphPad Prism 8.

716

717 **Isothermal titration calorimetry (ITC) analysis**

718 All reported isothermal titration calorimetry data were collected using a MicroCal ITC 200
719 instrument in the center of biomedical analysis, Tsinghua University. Ubc2 and all U2BR
720 peptides were buffer exchanged to 50 mM HEPES pH 7.5, and 150 mM NaCl before the
721 experiment. For the experiments, 20 μM Ubc2 solution in the sample cell was titrated with 400
722 μM U2BR peptide solution through 19 injections (2.0 μL each) at 25 °C and 750 rpm stirring
723 speed. Data fitting and analysis was performed using Origin 7 SR4 (OriginLab).

724

725 **REFERENCES**

726 1. Komander, D. & Rape, M. The Ubiquitin Code. *Annu. Rev. Biochem.* **81**, 203-229
727 (2012).
728 2. Yau, R. & Rape, M. The increasing complexity of the ubiquitin code. *Nat. Cell Biol.* **18**,
729 579-586 (2016).
730 3. Chau, V., Tobias, J. W., Bachmair, A., Marriott, D., Ecker, D. J., Gonda, D. K., &
731 Varshavsky, A. A Multiubiquitin Chain Is Confined to Specific Lysine in a Targeted Short-
732 Lived Protein. *Science* **243**, 1576-1583 (1989).
733 4. Chen, S.J., Wu, X., Wadas, B., Oh, J.H. & Varshavsky, A. An N-end rule pathway that
734 recognizes proline and destroys gluconeogenic enzymes. *Science* **355**, 6323 (2017).
735 5. Kim, J.M., Seok, O.H., Ju, S., Heo, J.E., Yeom, J., Kim, D.S., Yoo, J.Y., Varshavsky, A.,
736 Lee, C. & Hwang, C.S. Formyl-methionine as an N-degron of a eukaryotic N-end rule
737 pathway. *Science* **362**, eaat0174. (2018).
738 6. Tasaki, T., Sriram, S.M., Park, K.S. & Kwon, Y.T. The N-end rule pathway. *Annu. Rev.*
739 *Biochem.* **81**, 261-289 (2012).
740 7. Rusnac, D.V., Lin, H.C., Canzani, D., Tien, K.X., Hinds, T.R., Tsue, A.F., Bush, M.F.,
741 Yen, H.C.S. & Zheng, N. Recognition of the Diglycine C-End Degron by CRL2(KLHDC2)
742 Ubiquitin Ligase. *Mol. Cell* **72**, 813-822 (2018).
743 8. Varshavsky, A. The N-end rule pathway and regulation by proteolysis. *Protein Sci.* **20**,
744 1298-1345 (2011).
745 9. Zenker, M., Mayerle, J., Lerch, M. M., Tagariello, A., Zerres, K., Durie, P. R., ... & Reis,
746 A. Deficiency of UBR1, a ubiquitin ligase of the N-end rule pathway, causes pancreatic
747 dysfunction, malformations and mental retardation (Johanson-Blizzard syndrome). *Nat.*
748 *Genet.* **37**, 1345-1350 (2005).
749 10. Dougan, D.A. & Varshavsky, A. Understanding the Pro/N-end rule pathway. *Nat. Chem.*
750 *Biol.* **14**, 415-416 (2018).
751 11. Hwang, C.S., Shemorry, A., Auerbach, D. & Varshavsky, A. The N-end rule pathway is
752 mediated by a complex of the RING-type Ubr1 and HECT-type Ufd4 ubiquitin ligases.
753 *Nat. Cell Biol.* **12**, 1177-1185 (2010).
754 12. Tasaki, T., Zakrzewska, A., Dudgeon, D. D., Jiang, Y., Lazo, J. S., & Kwon, Y. T. The
755 substrate recognition domains of the N-end rule pathway. *J. Biol. Chem.* **284**, 1884-1895
756 (2009).
757 13. Upadhyay, A., Joshi, V., Amanullah, A., Mishra, R., Arora, N., Prasad, A., & Mishra, A.
758 E3 Ubiquitin Ligases Neurobiological Mechanisms: Development to Degeneration. *Front.*
759 *Mol. Neurosci.* **10**, 151 (2017).
760 14. Bartel, B., Wunning, I. & Varshavsky, A. The recognition component of the N-end rule
761 pathway. *EMBO. J.* **9**, 3179-3189 (1990).
762 15. Bodnar, N.O. & Rapoport, T.A. Molecular Mechanism of Substrate Processing by the
763 Cdc48 ATPase Complex. *Cell* **169**, 722-735 (2017).
764 16. Verma, R., Mohl, D. & Deshaies, R.J. Harnessing the Power of Proteolysis for Targeted
765 Protein Inactivation. *Mol. Cell* **77**, 446-460 (2020).
766 17. Burslem, G.M. & Crews, C.M. Proteolysis-Targeting Chimeras as Therapeutics and
767 Tools for Biological Discovery. *Cell* **181**, 102-114 (2020).
768 18. Pan, M., Gao, S., Zheng, Y., Tan, X., Lan, H., Tan, X., Sun, D., Lu, L., Wang, T., Zheng,
769 Q. and Huang, Y., Wang, J. & Liu, L. Quasi-Racemic X-ray Structures of K27-Linked
770 Ubiquitin Chains Prepared by Total Chemical Synthesis. *J. Am. Chem. Soc.* **138**, 7429-
771 7435 (2016).
772 19. Petroski, M.D. & Deshaies, R.J. Mechanism of lysine 48-linked ubiquitin-chain synthesis
773 by the cullin-RING ubiquitin-ligase complex SCF-Cdc34. *Cell* **123**, 1107-1120 (2005).

774 20. Saha, A. & Deshaies, R.J. Multimodal Activation of the Ubiquitin Ligase SCF by Nedd8
775 Conjugation. *Mol. Cell* **32**, 21-31 (2008).
776 21. Baek, K., Krist, D. T., Prabu, J. R., Hill, S., Klügel, M., Neumaier, L. M., ... & Schulman,
777 B. A. NEDD8 nucleates a multivalent cullin-RING-UBE2D ubiquitin ligation assembly.
778 *Nature* **578**, 461-466 (2020).
779 22. Horn-Ghetko, D., Krist, D. T., Prabu, J. R., Baek, K., Mulder, M. P., Klügel, M., ... &
780 Schulman, B. A Ubiquitin ligation to F-box protein targets by SCF-RBR E3-E3 super-
781 assembly. *Nature* **590**, 671-676 (2021).
782 23. Zivanov, J., Nakane, T., Forsberg, B. O., Kimanius, D., Hagen, W. J., Lindahl, E., &
783 Scheres, S. H. New tools for automated high-resolution cryo-EM structure determination
784 in RELION-3. *Elife* **7**, e42166 (2018).
785 24. Matta-Camacho, E., Kozlov, G., Li, F.F. & Gehring, K. Structural basis of substrate
786 recognition and specificity in the N-end rule pathway. *Nat. Struct. Mol. Biol. 17, 1182-*
787 *1187 (2010).*
788 25. Pfab, J., Phan, N.M. & Si, D. DeepTracer for fast de novo cryo-EM protein structure
789 modeling and special studies on CoV-related complexes. *Proc. Natl. Acad. Sci. USA*
790 **118**, e2017525118 (2021).
791 26. Emsley, P. & Cowtan, K. Coot: model-building tools for molecular graphics. *Acta.*
792 *Crystallogr. D. Biol. Crystallogr.* **60**, 2126-32 (2004).
793 27. Adams, P. D., Afonine, P. V., Bunkóczi, G., Chen, V. B., Davis, I. W., Echols, N., ... &
794 Zwart, P. H. PHENIX: a comprehensive Python-based system for macromolecular
795 structure solution. *Acta. Crystallogr. D. Biol. Crystallogr.* **66**, 213-221 (2010).
796 28. Chang, L., Zhang, Z., Yang, J., McLaughlin, S.H. & Barford, D. Atomic structure of the
797 APC/C and its mechanism of protein ubiquitination. *Nature* **522**, 450-454 (2015).
798 29. Brown, N.G., VanderLinden, R., Watson, E.R., Weissmann, F., Ordureau, A., Wu, K.P.,
799 Zhang, W., Yu, S., Mercredi, P.Y., Harrison, J.S. and Davidson, I.F. … & Schulman, B.A.
800 Dual RING E3 Architectures Regulate Multiubiquitination and Ubiquitin Chain Elongation
801 by APC/C. *Cell* **165**, 1440-1453 (2016).
802 30. Rusnac, D.V. & Zheng, N. Structural Biology of CRL Ubiquitin Ligases. *Adv. Exp. Med.*
803 *Biol.* **1217**, 9-31 (2020).
804 31. Waterhouse, A. Bertoni, M., Bienert, S., Studer, G., Tauriello, G., Gumienny, R., ... &
805 Schwede, T. SWISS-MODEL: homology modelling of protein structures and complexes.
806 *Nucleic. Acids. Res.* **46**, W296-W303 (2018).
807 32. Holm, L. DALI and the persistence of protein shape. *Protein Sci.* **29**, 128-140 (2020).
808 33. Du, F.Y., Navarro-Garcia, F., Xia, Z.X., Tasaki, T. & Varshavsky, A. Pairs of dipeptides
809 synergistically activate the binding of substrate by ubiquitin ligase through dissociation of
810 its autoinhibitory domain. *Proc. Natl. Acad. Sci. USA* **99**, 14110-14115 (2002).
811 34. Das, R., Mariano, J., Tsai, Y. C., Kalathur, R. C., Kostova, Z., Li, J., ... & Weissman, A.
812 M. Allosteric activation of E2-RING finger-mediated ubiquitylation by a structurally
813 defined specific E2-binding region of gp78. *Mol. Cell* **34**, 674-685 (2009).
814 35. Metzger, M. B., Liang, Y. H., Das, R., Mariano, J., Li, S., Li, J., ... & Weissman, A. M. A
815 Structurally Unique E2-Binding Domain Activates Ubiquitination by the ERAD E2,
816 Ubc7p, through Multiple Mechanisms. *Mol. Cell* **50**, 516-527 (2013).
817 36. Zheng, Q., Wang, T., Chu, G. C., Zuo, C., Zhao, R., Sui, X., ... & Liu, L. An E1-Catalyzed
818 Chemoenzymatic Strategy to Isopeptide-N-Ethylated Deubiquitylase-Resistant Ubiquitin
819 Probes. *Angew. Chem. Int. Ed. Engl.* **59**, 13496-13501 (2020).
820 37. Koliopoulos, M.G., Esposito, D., Christodoulou, E., Taylor, I.A. & Rittinger, K. Functional
821 role of TRIM E3 ligase oligomerization and regulation of catalytic activity. *Embo J.* **35**,
822 1204-1218 (2016).
823 38. Zheng, N. & Shabek, N. Ubiquitin Ligases: Structure, Function, and Regulation. *Annu.*
824 *Rev. Biochem.* **86**, 129-157 (2017).

39. Streich, F.C., Jr. & Lima, C.D. Capturing a substrate in an activated RING E3/E2-SUMO complex. *Nature* **536**, 304-308 (2016).
40. Xia, Z., Webster, A., Du, F., Piatkov, K., Ghislain, M., & Varshavsky, A. Substrate-binding sites of UBR1, the ubiquitin ligase of the N-end rule pathway. *J. Biol. Chem.* **283**, 24011-24028 (2008).
41. Pan, M., Zheng, Q., Ding, S., Zhang, L., Qu, Q., Wang, T., ... & Liu, L. Chemical Protein Synthesis Enabled Mechanistic Studies on the Molecular Recognition of K27-linked Ubiquitin Chains. *Angew. Chem. Int. Ed. Engl.* **58**, 2627-2631 (2019).
42. Qu, Q., Pan, M., Gao, S., Zheng, Q. Y., Yu, Y. Y., Su, J. C., ... & Hu, H. G. A Highly Efficient Synthesis of Polyubiquitin Chains. *Adv Sci (Weinh)* **5**, 1800234 (2018).
43. Zheng, S. Q., Palovcak, E., Armache, J. P., Verba, K. A., Cheng, Y., & Agard, D. A. MotionCor2: anisotropic correction of beam-induced motion for improved cryo-electron microscopy. *Nat. Methods* **14**, 331-332 (2017).
44. Mindell, J.A. & Grigorieff, N. Accurate determination of local defocus and specimen tilt in electron microscopy. *J. Struct. Biol.* **142**, 334-47 (2003).
45. Pettersen, E.F. et al. UCSF ChimeraX: Structure visualization for researchers, educators, and developers. *Protein Sci.* **30**, 70-82 (2021).
46. Krissinel, E. & Henrick, K. Inference of macromolecular assemblies from crystalline state. *J. Mol. Biol.* **372**, 774-797 (2007).